

Verifying Operational Forecasts of Land-Sea Breeze and Boundary Layer

Mixing Processes

Ewan Short*

*School of Earth Sciences, and ARC Centre of Excellence for Climate Extremes, The University of
Melbourne, Melbourne, Victoria, Australia.*

Ben ?. Price

Bureau of Meteorology, Casuarina, Northern Territory, Australia

Derryn ?. Griffiths and Alexei ?. Hider

Bureau of Meteorology, Melbourne, Victoria, Australia

*Corresponding author address: School of Earth Sciences, The University of Melbourne, Melbourne, Victoria, Australia.

E-mail: shorte1@student.unimelb.edu.au

ABSTRACT

13 This study presents a method for verifying the diurnally varying compo-
14 nent of operational wind forecasts that are typically based on model data that
15 is then edited by human forecasters. The model datasets most commonly
16 used by Australian forecasters for winds are those of the European Center
17 for Medium-Range Weather Forecasting (ECMWF) and the Australian Com-
18 munity Climate and Earth System Simulator (ACCESS). The methodology is
19 applied to the coastal weather stations across Australia over June, July and
20 August 2018, at three different spatial scales, on both a daily and seasonal ba-
21 sis. The results indicate that while the Official forecast outperforms unedited
22 ACCESS and ECMWF at certain locations and times of day, it rarely outper-
23 forms both at once. The causes of the differences in the performance of each
24 dataset vary by location, but can include biases in the direction at which the
25 sea-breeze approaches the coast, amplitude biases in the diurnal cycle, and
26 disagreement as to whether sea-breeze or boundary layer mixing processes
27 contribute most to the diurnal cycle. Furthermore, when winds are compared
28 at small spatial scales on a daily basis, ECMWF outperforms Official and
29 ACCESS simply because its coarser resolution creates less internal variability
30 than Official or ACCESS. These results have implications for both forecasting
31 practice and verification methodology.

32 1. Introduction

33 Modern weather forecasts are typically produced by models in conjunction with human fore-
34 casters. Forecasters working for the Australian Bureau of Meteorology (BoM) construct a seven
35 day forecast by loading model data into a software package called the Graphical Forecast Editor
36 (GFE), then editing this model data using tools within GFE. Is this also how things work at the
37 U.S National Weather Service and U.K. Met Office? Forecasters can choose which model to base
38 their forecast on, and refer to this as a choice of *model guidance*. Edits are typically made to
39 account for processes that are under-resolved at synoptic scale model resolutions, or to correct
40 known biases of the models being used. The resulting gridded forecast datasets are then provided
41 to the public through the BoM's online MetEye data browser (Bureau of Meteorology 2019); the
42 gridded forecast datasets are also translated into text and icon forecasts algorithmically.

43 Australian forecasters generally make two types of edits to the surface wind fields on a routine
44 daily basis. The first is to edit the surface winds after sunrise at locations where the forecaster be-
45 lieves the model guidance is providing a poor representation of boundary layer mixing processes.
46 Boundary layer mixing occurs as the land surface heats up, producing an unstable boundary layer
47 which transports momentum downward to the surface layer, where winds are both weaker and
48 ageostrophically oriented due to surface friction (Lee 2018). The forecaster may edit both speed
49 and direction on the basis of climatological knowledge, theory or recent upper level wind sound-
50 ings from nearby stations. How do the boundary layer mixing tools in GFE currently work? While
51 I was in Darwin you picked a height z and a percentage p , and the tool essentially formed an aver-
52 age of the surface winds and winds at x weighted by p .

53 The second type of edit involves changing the afternoon and evening surface winds around those
54 coastlines where the forecaster believes the model guidance is resolving the sea-breeze poorly.

55 How do the sea-breeze tools in GFE currently work? While I was in Darwin you traced out the
56 relevant coastline graphically, chose a wind speed and a time, and GFE would add in winds perpen-
57 dicular to the traced coastline at this speed, and smoothly blend them in spatially and temporally.

58 Forecasters and national weather services have good reasons for ensuring the diurnally varying
59 component of their wind forecasts are as accurate as possible. Dai and Deser (1999) fitted the first
60 two harmonics to seasonal averages of wind speed at different times of day and showed that over
61 land surfaces the average amplitude of the wind speed diurnal cycle varied from 1.2 to 2.1 kn,
62 (knots are used throughout this paper because this is the unit forecasters work with, and the unit
63 that is used in Jive) and that the fitted harmonics accounted for 50 to 70% of the daily variability.
64 Table 1 shows the mean wind speeds for the Australian capital city airport station shown in Fig. 1,
65 over December, January, February 2017/18 and June, July and August 2018, suggesting that the
66 amplitude of the mean diurnal cycles are approximately 10 to 34% of the mean wind speeds across
67 Australia.

68 Beyond their contribution to the overall wind field, diurnal wind cycles are important in and of
69 themselves to the ventilation of pollution, with sea-breezes transporting clean maritime air inland,
70 where it helps flush polluted air out of the boundary layer (Miller et al. 2003). The Victorian
71 Latrobe Valley provides an important Australian example of this effect (Physick and Abbs 1992).
72 Furthermore, diurnal wind cycles affect the function of wind turbines (Englberger and Dörnbrack
73 2018) and the design of wind farms (Abkar et al. 2016), as daily patterns of boundary layer stability
74 affect turbine wake turbulence, and the losses in wind power that result.

75 To our knowledge, no published work has assessed the diurnal component of human edited
76 forecasts, although some previous studies have assessed the performance of different operational
77 models at specific locations. Svensson et al. (2011) examined thirty different operational model
78 simulations, including models from most major forecasting centres utilising most commonly used

79 boundary layer parametrisation schemes, and compared their performance with a large eddy sim-
80 ulation (LES), and observations at Kansas, USA during October 1999. They found that both the
81 models and LES failed to capture the sudden ≈ 6 kn jump in wind speeds shortly after sunrise,
82 and underestimated morning low level turbulence and wind speeds. Other studies have assessed
83 near-surface wind forecasts, verifying the total wind speeds, not just the diurnal component. Pin-
84 son and Hagedorn (2012) performed a verification study of the 10 m wind speeds resolved by the
85 European Centre for Medium Range Weather Forecasting (ECMWF) operational model ensemble
86 across western Europe over December, January, February 2008/09. They found that the worst per-
87 forming regions were coastal and mountainous areas, and attributed this poor performance to the
88 small scale processes, e.g. sea and mountain breezes, that are under-resolved at ECMWF's coarse
89 50km spatial resolution.

90 Any attempt to validate model data against observations must confront the *representation prob-*
91 *lem* (e.g. Zaron and Egbert 2006). Because models cannot resolve physical processes occurring at
92 sub-grid scales, a value predicted by an operational model for a given grid-cell must be interpreted
93 as a prediction of the filtered, or Reynolds averaged value over that grid-cell. While strictly speak-
94 ing, observational instruments also impose a degree of filtering on reality, in the case of the AWS
95 observations considered here, the filtering is much less than for the model predictions. Therefore,
96 comparing model data with observational data can be an unfair test of model performance, and for
97 this reason model forecasts are often verified against reanalysis hind-casts that use the same model
98 (e.g. Lynch et al. 2014).

99 However, the way the representation problem applies to the verification of forecasts issued to the
100 public is more nuanced. In this case, a forecast issued by a national weather service is attempting
101 to represent either reality itself, or the filtered version of reality *that is of interest to the end user*.
102 Thus, Pinson and Hagedorn (2012) disregarded the representation problem entirely, arguing that

103 the end user is not interested in spatiotemporal scales of models, only the best representation of
104 reality at the time and place of their choice. However, it is hard (impossible) to completely es-
105 cape making assumptions about the filtered version of reality the end user wants from a forecast.
106 BoM wind verification scores used internally are derived by comparing hourly Official forecast
107 data with station observations that are averaged 10 minutes either side of the hour: implicit in this
108 practice is the assumption that the user does not care about wind turbulence at temporal scales less
109 than 20 minutes. Beyond this, the fact that the Official forecast is formed from model datasets
110 with different resolutions, with the choice of model guidance changing over the course of a single
111 day, e.g. Fig. ?? c), makes the precise version of reality the Official forecast is intending to rep-
112 resent unclear, and hence addressing the representation problem difficult. The point I'm trying to
113 make here is perhaps unclear. Essentially I'm arguing that the representation problem applies, but
114 although the intended filtered version of reality represented by a particular model is clear, it is not
115 clear in the Official forecast due to its hybrid structure, and because what it intends to represent is
116 perhaps not clear to the user, or consistent between different users. Note that clicking locations on
117 the MetEye map seems to bring up the forecast for the nearest station or population centre. Does
118 this imply that the Official forecast is intending to represent spatial scales at least as fine as the
119 distance between stations? Or is it intending to represent averaged parameters at the ACCESS-R
120 or ACCESS-C resolutions? Note also that grids are only provided every 3 hours in MetEye; do
121 these grids represent the hourly values from the Official forecast, provided just at these three hour
122 intervals, or a three hourly average?

123 Related to the representation problem is the question of how mesoscale models, which run at
124 spatial resolutions of between 1 and 10 km, should be verified. This question is of relevance to
125 the present study as the BoM now regularly runs mesoscale models over some Australian capital
126 cities as part of its daily forecasting routine, and the edits performed by human forecasters are also

127 often performed at the mesoscale. Mesoscale models resolve topography and its effects on the
128 atmosphere in more detail, and explicitly simulate most convective and boundary layer processes.
129 In this sense they are more realistic than coarser scale synoptic models, although they can actually
130 perform worse than coarse models on standard verification scores whenever there are timing or
131 location differences between features in the models and in observations. Mass et al. (2002) found
132 that in the northwestern United States, mean square error scores in forecasts produced using a
133 mesoscale model decreased with resolution down to 10 to 15 km, whereas in the eastern United
134 States where the topography is much flatter, this threshold was considerably larger, at 20 to 40 km.

135 Mass et al. (2002) therefore argued that existing verification approaches needed reform, suggest-
136 ing that verification could instead be performed on spatially or temporally averaged parameters,
137 an approach now known as *upscaling* (Ebert 2008), or that “feature based” identification metrics
138 be developed, which reward models for realistically simulating atmospheric features, even if the
139 timing or location of these features is slightly incorrect. Ebert and McBride (2000) developed such
140 a method for precipitation, focusing on spatial displacements and differences in the shapes of the
141 rainfall areas between observations and models. Rife and Davis (2005) applied similar ideas to the
142 verification of surface winds, defining a wind “object” as a wind change of at least one standard
143 deviation occurring within a 12 hour interval, then assessing whether a mesoscale model could
144 replicate the “objects” present in observations.

145 The present study has two goals. First, to describe a method for comparing the diurnal cycles
146 of human edited wind forecasts to those of unedited model guidance forecasts, in order to assess
147 where and when human edits produce an increase in accuracy, and to do so in a way that re-
148 spects the representation and mesoscale verification challenges discussed above. Second, to apply
149 this methodology across Australian coastal locations to better understand the performance of both
150 boundary layer mixing and land-sea breeze forecaster edits. The remainder of this paper is organ-

151 ised as follows. Section 2 describes the methodology and datasets to which it is applied, section 3
152 provides results, and sections 4 and 5 provide a discussion and a conclusion, respectively.

153 **2. Data and Methods**

154 This study compares both human edited and non human edited Australian Bureau of Meteorol-
155 ogy wind forecasts with automatic weather station (AWS) data across Australia. The comparison
156 is performed by first isolating the diurnal signals of each dataset, then comparing these signals
157 on an hour-by-hour basis. Much of the analysis is conducted through the BoM's *Jive* verification
158 platform (Provide either a URL link to an Official Jive page if one exists by the time of publica-
159 tion, or a link to copy of Jive I've been using on my laptop, which I could host on my personal
160 GitHub page.), which provides an archive of forecast, model guidance and observational data, and
161 a software library for calculating basic statistics.

162 *a. Data*

163 Four datasets are considered in this study; the Official BoM wind forecast data that is issued to
164 the public, model data from ECMWF, (is this the mean of the ECMWF operational ensemble?)
165 model data from the Australian Community Climate and Earth System Simulator (ACCESS), (I
166 haven't considered the BoM's Operational Consensus Forecast in this study, because it was not
167 used in the Official forecast for winds while I was in the NT. If it is used in other states, the study
168 can be reinterpreted as a verification of both forecaster edits and OCF against unedited, un-post-
169 processed model guidance.) and observational data from automatic weather stations (AWS) across
170 Australia. (With the Bureau's permission, I would like to make the datasets used in this paper open
171 access, and host them on the NCI catalogue page.) The Official and ECMWF data are at a ?, ?
172 degree spatial resolution respectively. What are the resolutions of these datasets as they're used in

173 Jive? I know ACCESS uses nested grids, so what is the resolution of the ACCESS dataset when
174 used in GFE and Jive? Are the outer grids interpolated to the resolution of the inner grids, or are
175 the inner grids upscaled? Official, ACCESS and AWS data exists at each UTC hour, but ECMWF
176 data only exists at a three hour resolution. Why is this? What are the actual time-steps of the
177 models? To be consistent with the other data sets, ECMWF is therefore linearly interpolated to
178 an hourly resolution: note that this is also what happens when forecasters load ECMWF wind
179 data into the GFE, and the linearly-interpolated ECMWF data is therefore an appropriate model
180 guidance dataset to compare with Official. To facilitate comparison with observations, Official,
181 ACCESS and ECMWF data is (tri-linearly?) interpolated in all three spatial dimensions to the
182 locations of the weather stations. AWS wind data is recorded every minute at each station, and
183 the hourly AWS datasets used in Jive for this study, and all other internal BoM wind verification
184 studies, are formed by averaging 10 minutes either side of each UTC hour. (My memory is that
185 Jive uses a ten minute average either side, but need to confirm this as it could be five minutes either
186 side.)

187 Both ACCESS and ECMWF use parametrisation schemes to simulate sub-grid scale boundary
188 layer turbulence, and the resultant mixing. ACCESS uses the schemes of Lock et al. (2000) and
189 Louis (1979) for unstable and stable boundary layers respectively (Bureau of Meteorology 2010).
190 ECMWF uses similar schemes that they develop in-house (European Center for Medium Range
191 Weather Forecasting 2018). Data covers the austral winter months of June, July and August 2018;
192 this short time period was chosen to reduce the effect of changing seasonal and climatic conditions,
193 changing forecasting practice and staff, and of developments to the ACCESS and ECMWF models.

194 *b. Assessing Diurnal Cycles*

195 The overall surface diurnal wind signal includes land-sea breezes, boundary layer mixing pro-
 196 cesses, mountain-valley breezes, atmospheric tides, and urban heat island circulations. Forecasters
 197 typically edit model output to account for under-resolved sea-breezes and boundary layer mixing
 198 processes. Instead of attempting to assess each type of edit individually, we study the overall di-
 199 urnal signal by subtracting a twenty hour centred running mean *background wind* from each zonal
 200 and meridional hourly wind data point. This provides a collection of zonal and meridional wind
 201 *perturbation* datasets.

202 One measure of the accuracy of the Official, ACCESS and ECMWF diurnal cycles is to com-
 203 pare the Euclidean distances of the perturbations at each hour with the corresponding AWS per-
 204 turbations. For example, to assess whether the Official forecast perturbations, \mathbf{u}_O , or ACCESS
 205 perturbations, \mathbf{u}_A , best match the AWS observations, \mathbf{u}_{AWS} , we calculate the *Wind Perturbation*
 206 *Index* (WPI), defined by

$$\text{WPI}_{OA} = |\mathbf{u}_{AWS} - \mathbf{u}_A| - |\mathbf{u}_{AWS} - \mathbf{u}_O|. \quad (1)$$

207 The analogously defined quantities WPI_{OE} and WPI_{EA} can then be used to provide a comparison
 208 of the Official and ECMWF perturbations, and of the ACCESS and ECMWF perturbations, re-
 209 spectively. We can then take means of the WPI on an hourly basis; i.e. all the 00:00 UTC WPI
 210 values are averaged, all the 01:00 UTC values are averaged, and so forth, and denote such an
 211 average by $\overline{\text{WPI}}$.

212 $\overline{\text{WPI}}$ is the difference of two mean absolute errors. A $\overline{\text{WPI}}_{OA}$ value of 0.5 kn at 00:00 UTC
 213 means that the Official 00:00 UTC perturbations are, on average, 0.5 kn closer to the observed
 214 perturbations than are those of ACCESS. The WPI compares just *one aspect* of the Official forecast
 215 with model guidance; it says nothing, for instance, about whether the variability of the Official

216 forecast is closer to that of the AWS than the model guidance. As such, any statements about
217 performance made throughout this paper refer solely to WPI, and no claim is being made that WPI
218 is sufficient to completely characterise the accuracy, or value to the user, of how the surface diurnal
219 wind cycle is represented in competing forecasts.

220 Note that sea-breeze and boundary layer mixing processes depend crucially on the background
221 atmospheric conditions in which they occur. By comparing wind perturbations rather than the
222 overall wind fields we are not claiming these background conditions are irrelevant. However,
223 when a forecaster makes an edit of a wind forecast to better resolve these processes, they are
224 implicitly assuming that future background conditions will be close enough to either climatology,
225 or model predictions of background conditions themselves, to justify making the edit. Thus, it
226 makes perfect sense to compare forecast perturbations to observed perturbations, as long as errors
227 are interpreted as the consequence not only of how the forecaster or model resolves the diurnal
228 cycle, but of how errors in the background state contribute to errors in the perturbations. To
229 minimise the significance of background state errors, this study focuses exclusively on lead-day
230 one forecasts.

231 Given the large degree of turbulence and unpredictable variability in both the AWS, Official,
232 and model datasets, care must be taken to ensure we do not pre-emptively conclude Official has
233 outperformed the model guidance when $\overline{\text{WPI}} > 0$ purely by chance. The method for estimating
234 confidence in $\overline{\text{WPI}}$ is based on a method proposed by Griffiths et al. (2017) as a general frame-
235 work for BoM verification metrics. Note first that WPI is defined so as to minimise the temporal
236 autocorrelations within each dataset, and to avoid having to consider correlations between the
237 zonal and meridional components within and between datasets. Time series formed from the WPI
238 values at a particular time, say 00:00 UTC, across the three month time period, can therefore be
239 idealised as an independent random sample of a random variable W . The sampling distribution for

each \overline{WPI} can be modelled by a Student's t -distribution, and from this we calculate the probability
 that W is positive, denoted $\Pr(W > 0)$. Although temporal autocorrelations of WPI, i.e. corre-
 lations between WPI values at a particular hour from one day to the next, are in practice small
 or non-existent thanks to how WPI is defined, they are still accounted for by reducing the “ef-
 fective” sample size to $n(1 - \rho_1) / (1 + \rho_1)$, where n is the actual sample size and ρ_1 is the lag-1
 autocorrelation (Zwiers and von Storch 1995; Wilks 2011). Note that in the standard language of
 statistical hypothesis testing, we would reject the null hypothesis that $W = 0$ at significance level
 α if $\Pr(W > 0) > 1 - \frac{\alpha}{2}$ or $\Pr(W < 0) > 1 - \frac{\alpha}{2}$. However, in this study we are interested in both
 whether $W > 0$ or whether $W < 0$, so prefer to simply state the value of $\Pr(W > 0)$, referring to
 this as a *confidence score*, and noting $\Pr(W < 0) = 1 - \Pr(W > 0)$. We say Official outperforms
 model guidance with “high confidence” if $\Pr(W > 0) \geq 95\%$, or that model guidance outperforms
 Official with “high confidence” if $\Pr(W > 0) \leq 5\%$, with high confidence implicit whenever it is
 not explicitly mentioned. **Much of this explanation is probably unnecessary, but would like to get
 feedback before I trim it.**

To investigate the consequences of the representation and mesoscale verification challenges dis-
 cussed in section 1, we apply *upscaling* (Ebert 2008), where forecast and observational data are
 first averaged to coarser spatiotemporal scales before being compared. In this study we consider
 three spatial and two temporal scales. The finest spatial scale is that of the individual station.
 This study focuses on the 8 capital city airport stations, marked by stars in Fig. 1, as their high
 operational significance means that they are typically the most accurate and well maintained. The
 next spatial scale is formed by taking the 10 stations closest to each capital city airport station,
 with some flexibility allowed to ensure stations are roughly parallel to the nearest coastline. These
 station groups are referred to as the *airport station groups*. The coarsest spatial scale is formed
 by taking all stations within 150 km of the nearest coastline, and grouping these by state. This is

done because Australian forecasts are currently produced on a state by state basis at forecasting centres based in each state capital, with each forecasting centre utilising different staff, different model guidance preferences, and different editing practices. Indeed, the Official gridded forecast typically shows slight discontinuities across state boundaries (Bureau of Meteorology 2019). Note that the Western Australian coastline is subdivided into three pieces, and stations along the Gulf of Carpentaria, north Queensland Peninsula, and Tasmanian coastlines are neglected, in order to ensure each station group corresponds to an approximately linear segment of coastline, so as to best resolve the land-sea breeze signal after spatial averaging (e.g. Vincent and Lane 2016). These eight station groups are referred to as the *coastal station groups*.

We also consider both daily and seasonal time scales. For daily time scales, we either consider just the individual airport stations, or modify the definition of WPI in equation (1) so that each perturbation dataset is first spatially averaged over either the airport or coastal station groups. Confidence scores are calculated for the airport and coastal station groups in the same way as for the single airport stations, treating the spatially averaged data as a single time series. This provides a conservative way to deal with spatial correlation between the stations in each group (Griffiths et al. 2017).

For the seasonal scale comparison we define the *Climatological Wind Perturbation Index* (CWPI) by

$$\text{CWPI}_{\text{OA}} = |\overline{\mathbf{u}}_{\text{AWS}} - \overline{\mathbf{u}}_{\text{O}}| - |\overline{\mathbf{u}}_{\text{AWS}} - \overline{\mathbf{u}}_{\text{A}}|, \quad (2)$$

where the over-bars denote temporal averages of the perturbations at a particular hour, across the three month time period. These temporally averaged perturbations represent the climatological diurnal wind cycle over the three month study period for each dataset. As with the WPI, CWPI_{OE} and CWPI_{EA} are defined analogously. The three spatial scales are considered in the same way as for WPI, with the spatial average taken before the temporal average. Note that the upscaling

method provides another motivation for considering perturbations rather than the overall wind fields, as this prevents the averaged diurnal cycles being washed out by larger scale variability. Uncertainty in the CWPI is estimated through bootstrapping (Efron 1979). This is done by performing resampling with replacement on the underlying perturbation datasets, and calculating the CWPI multiple times using these resampled datasets. This provides a distribution of CWPI values, which analogously to with WPI, we treat as a sample from a random variable C , and use this to estimate $\Pr(C > 0)$.

Although the WPI and CWPI provide quantitative information on the accuracy of the diurnal cycle at different times of day, they do not provide much information on the structure of the diurnal wind cycles of each dataset. Gille et al. (2005) obtained summary statistics on the observed structure of the climatological diurnal wind cycles across the globe by using linear regression to calculate the coefficients u_i, v_i $i = 0, 1, 2$, for the fits

$$u = u_0 + u_1 \cos(\omega t) + u_2 \sin(\omega t), \quad (3)$$

$$v = v_0 + v_1 \sin(\omega t) + v_2 \cos(\omega t), \quad (4)$$

where ω is the angular frequency of the earth and t is the local solar time in seconds. If a temporal hodograph of this fit is considered, i.e. if (u, v) are plotted in an x, y plane for different values of t , the tips of the vectors trace out an ellipse. Gille et al. (2005) used this to calculate descriptive quantities, like the eccentricity of the ellipse, and the angle the semi-major axis of the ellipse makes with the horizontal, directly from the coefficients u_1, u_2, v_1 and v_2 . Gille et al. (2005) applied this fit to scatterometer data, which after temporal averaging resulted in just four zonal and meridional values per location, and as such the fit performed very well.

However, equations (3) and (4) do not provide a good fit for hourly wind data, primarily because they assume a twelve hour symmetry in the evolution of the diurnal cycle. In practice, asymmetries

308 between daytime heating and nighttime cooling (e.g. Svensson et al. 2011) result in surface wind
 309 perturbations accelerating rapidly just after sunrise, but remaining comparatively stagnant at night
 310 (e.g. Fig. 9). Thus, we instead fit the equations

$$u = u_0 + u_1 \cos(\alpha(\psi, t)) + u_2 \sin(\alpha(\psi, t)), \quad (5)$$

$$v = v_0 + v_1 \sin(\alpha(\psi, t)) + v_2 \cos(\alpha(\psi, t)), \quad (6)$$

311 to the climatological perturbations, with α the function from $[0, 24) \times [0, 2\pi) \rightarrow [0, 2\pi)$ given by

$$\alpha(\psi, t) \equiv \pi \left[\sin \left(\pi \frac{(t - \psi) \bmod 24}{24} - \frac{\pi}{2} \right) + 1 \right], \quad (7)$$

312 with t the time in units of hours UTC, and ψ providing the time when the wind perturbations vary
 313 least with time. For each climatological diurnal wind cycle, we solve for the seven parameters u_0 ,
 314 u_1 , u_2 , v_0 , v_1 , v_2 and ψ using nonlinear regression, performed using the `least_squares` function
 315 from the `scipy.optimize` python module (SciPy 2019).

316 Note Gille et al. (2005) fit equations (3) and (4) to the temporally averaged wind fields, so that
 317 (u_0, v_0) could be interpreted as the mean wind over the study's time period, and the remaining
 318 terms providing the climatological diurnal perturbations. In this study we fit equations (5) and
 319 (6) to the climatological perturbations, with (u_0, v_0) now necessary to offset the asymmetry intro-
 320 duced by α , i.e. to ensure the time integral of the fitted perturbation values is approximately zero.
 321 Following Gille et al. (2005), the ellipse's orientation, i.e. the angle the semi-major axis of the el-
 322 lipse makes with lines of latitude, as well as the ellipse's eccentricity are calculated algebraically,
 323 but the perturbation speed maximum, and the time at which this maximum achieved, are instead
 324 obtained numerically.

3. Results

In this section, the methods described in section 2 are applied to Australian forecast and station data over the months of June, July and August (austral winter) 2018. First, differences are assessed on a daily basis using the Wind Perturbation Index (WPI) at three different spatial scales. Second, overall seasonal biases during this time period are assessed using the Climatological Wind Perturbation Index (CWPI), and by comparing structural indices derived from ellipses fitted to the climatological wind perturbations.

a. Daily Comparison

Figure 2 provides the WPI values and confidence scores for the coastal station groups for $\overline{\text{WPI}}_{\text{OA}}$, $\overline{\text{WPI}}_{\text{OE}}$ and $\overline{\text{WPI}}_{\text{EA}}$, which represent the Official versus ACCESS, Official versus ECMWF, and ECMWF versus ACCESS comparisons, respectively. The results indicate that for the majority of station groups and hours, both the unedited ACCESS and ECMWF models outperform the Official forecast. The lowest $\overline{\text{WPI}}$ values occur at the NT station group at 23:00 and 00:00 UTC for both $\overline{\text{WPI}}_{\text{OA}}$ and $\overline{\text{WPI}}_{\text{OE}}$. Although Official outperforms at least one of ACCESS or ECMWF at multiple times and station groups, the only group and time where it outperforms both is 05:00 UTC over the South WA station group, although the $\overline{\text{WPI}}$ values are comparatively low. ECMWF generally outperforms ACCESS from 10:00 - 14:00 UTC, with the South WA station group being the main exception.

Figures 3 and 4 provide case studies of the NT and South WA station groups, respectively. Figure 3 a) provides a time series of WPI for the NT station group at 23:00 UTC. The time series shows significant temporal variability, with WPI frequently exceeding -2 kn. **The time series in Figures 3 and 4 are perhaps unnecessary, but I included them because they show both variability, and the lack of temporal autocorrelation in WPI.** Figures 3 b) and c) show hodographs of the winds

348 and wind perturbations, respectively, for the AWS observations, Official forecast, and ACCESS
349 and ECMWF model datasets, at each hour UTC on the 3rd of July, which provides an interesting
350 example.

351 Figure 3 b) shows that the Official wind forecast on this day was likely based on edited ACCESS
352 from 00:00 to 06:00 UTC, then edited ECMWF from 07:00 to 13:00 UTC, then unedited ACCESS
353 from 15:00 to 21:00 UTC. The final two hours of the forecast show the Official winds acquiring a
354 stronger east-northeasterly component than either the AWS observations, ACCESS, or ECMWF.
355 This rapid change is clearer in the perturbation hodograph shown in Fig. 3 c). At this time of
356 year the prevailing winds throughout the NT are east-southeasterly, and 22:00 UTC corresponds
357 to \approx 08:30 local solar time (LST) in this region, so the rapid departure of the Official forecast
358 from ACCESS at this time likely represents an edit made by a forecaster to capture boundary layer
359 mixing processes. Figure 5 a) shows the first ten values from wind soundings at Darwin Airport
360 at 12:00 UTC on July 3rd and 00:00 UTC on July 4th. In both instances the winds are indeed
361 east-southeasterly, and so the rapidly changing wind perturbations at 22:00 UTC in the Official
362 forecast likely reflect a boundary layer mixing edit that has been applied either too early, or has
363 strengthened the southeasterly component of the winds too much. Similar issues create low WPI
364 scores on the 8th of June and 9th and 10th of July.

365 Figure 4 a) provides a time series of WPI for the South WA station group at 05:00 UTC. As with
366 the NT station group there is significant temporal variability, with WPI frequently exceeding 1 kn.
367 Figures 4 b) and c) provides hodographs of the winds and wind perturbations, respectively, on the
368 9th of June, which is an interesting example. The perturbation hodograph shows both ECMWF
369 and ACCESS underpredicting the amplitude of the diurnal wind cycle on this day. In each dataset
370 the 05:00 UTC perturbations are westerly to northwesterly, and given the orientation of the South

371 WA coastline (see Fig. 1) and the fact that 05:00 UTC corresponds to $\approx 13:00$ local solar time
372 (LST) in this region, the perturbations likely indicate boundary layer mixing processes.

373 Figure 5 shows wind sounds throughout the first two km of the atmosphere between 12:00 UTC
374 on the 8th June and 12:00 UTC on the 9th June; the soundings were taken at Perth Airport, which
375 is the nearest station to the South WA station group to provide wind soundings. The 8th June 12:00
376 UTC sounding shows surface northerlies of ≈ 6 kn, becoming west to northwesterlies of over 20
377 kn 2.4 km above the surface. A forecaster basing a model edit of the following days winds on
378 this sounding would therefore gradually strengthen the westerly component of the surface winds
379 in the hours after sunrise. However, the subsequent sounding at 00:00 UTC on the 9th of June
380 shows that the winds acquire a strong northerly component of 30 kn in the first 500 m of the
381 atmosphere, with the final sounding indicating a strong northwesterly wind at 725 m persisting
382 until 12:00 UTC. In Fig. 4 c), the Official perturbations from 04:00 to 07:00 UTC show stronger
383 westerly perturbations than either ACCESS or ECMWF, improving the amplitude of Official's
384 diurnal wind cycle. However, the AWS perturbations are more northerly than those of Official,
385 and so the Official forecast winds have been strengthened in a slightly incorrect direction. One
386 explanation for this discrepancy is that the Official forecast has been edited based on the June 8th
387 12:00 UTC sounding, with the winds above the surface changing direction in the subsequent 12
388 hours. A similar explanation can be given for the high WPI scores on the 3rd of August, although
389 in this case the Official forecast slightly improves both the magnitude and direction of the 05:00
390 UTC wind perturbations.

391 To provide a contrast to the coastal station group results, Fig. 6 presents the $\overline{\text{WPI}}$ values and
392 confidence scores for $\overline{\text{WPI}}_{\text{OE}}$, which represents the Official versus ECMWF comparison, for the
393 airport stations, and airport station groups. The results for the airport stations are noisier than the
394 results for the coastal station groups in Figs. 2 c) and d), although they share some similarities.

395 Official outperforms ECMWF at 01:00 and 02:00 UTC at both the Darwin airport station and
396 the NT station group, although ECMWF outperforms Official between 08:00 and 14:00 UTC
397 at Darwin and Brisbane airports, and the corresponding NT and QLD station groups, with the
398 exception of the QLD station group at 12:00 UTC. ECMWF also outperforms Official at Hobart
399 airport at almost all hours of the day, and at Adelaide and Canberra airports from 11:00 to 14:00
400 UTC.

401 For the remaining stations and times, Official only outperforms ECMWF at the Perth airport
402 station at 06:00 UTC and the Melbourne airport station at 01:00 UTC, although in both cases WPI
403 values are comparatively small in magnitude. Furthermore, in both cases there is no clear pattern
404 to the \overline{WPI}_{OE} values over the rest of the day. Note that the *multiplicity problem* (Wilks 2011, p.
405 178) requires care be taken before giving meaning to these two examples: i.e., given that we are
406 calculating twenty four confidence scores for eight stations, then if WPI were uncorrelated across
407 each station and hour we would expect to find $0.05 \times 24 \times 8 \approx 10$ instances where $P(W_{OE} > 0) \geq$
408 95%, even if W_{OE} were in fact equal to zero.

409 For the airport station groups, ECMWF outperforms Official for the majority of station groups
410 and times. The main exception is the Darwin airport station group, where Official outperforms
411 ECMWF at 02:00 UTC, ambiguity as to whether Official or ECMWF performs better at 01:00,
412 03:00 and 04:00 UTC, and from 15:00 to 22:00 UTC. In the analogous \overline{WPI}_{OA} Official versus
413 ACCESS comparisons (not shown), the airport station results are similarly noisy, although the
414 airport station group results are slightly more favourable to Official, with Official outperforming
415 ACCESS from 10:00 to 12:00 UTC at the Brisbane station group, and fewer occasions overall
416 where ACCESS outperforms Official than ECMWF does.

417 Figure 7 presents the \overline{WPI} values and confidence scores for \overline{WPI}_{EA} , which represents the
418 ECMWF versus ACCESS comparison, for the airport stations, and airport station groups. As with

the Official versus ECMWF comparison in Fig. 6, the results for the airport stations are noisy, but more often than not show that ECMWF outperforms ACCESS. The results for the airport station group show ECMWF usually outperforms ACCESS, the main exceptions being the Darwin and Canberra airport station groups. Might be interesting to note that ACCESS-C+ does not run over Darwin or Canberra, possibly explaining the better performance of ACCESS there.

Naively, the fact that ECMWF generally outperforms ACCESS at these scales is surprising, as ACCESS runs at a higher spatiotemporal resolution than ECMWF, and is calibrated for Australian conditions. However, these results are not surprising in light of the mesoscale verification challenges discussed in section 1. The AWS data resolves motion with time scales as low as 10 minutes, and at arbitrarily small spatial scales: it therefore includes more unpredictable turbulence than either model dataset. Furthermore, because ACCESS runs at higher spatiotemporal resolutions than ECMWF, it includes additional scales of motion, and therefore adds additional variability to the wind fields. Unless the additional variability in ACCESS is perfectly correlated with observations, the average of $|\mathbf{u}_{\text{AWS}} - \mathbf{u}_{\text{A}}|$ will therefore increase, unless this additional variability is compensated for by a reduction in bias, i.e. $|\overline{\mathbf{u}}_{\text{AWS}} - \overline{\mathbf{u}}_{\text{A}}|$ decreases. These ideas are discussed in greater detail in section 4. Note finally that the results for the Official versus ECMWF comparison in Fig. 6 largely mirror those of the ECMWF versus ACCESS comparison in Fig. 7, suggesting that similar arguments apply to Official, as it is based on both ACCESS, ECMWF as well as forecaster edits, which contribute additional variability.

b. Seasonal Comparison

Figure 8 provides the Climatological Wind Perturbation Index (CWPI) values and confidence scores for the coastal station groups for CWPI_{OA} , CWPI_{OE} and CWPI_{EA} , which represent the Official versus ACCESS, Official versus ECMWF, and ECMWF versus ACCESS comparisons,

442 respectively. At the NT station group Official outperforms both ACCESS and ECMWF at 03:00
443 UTC with reasonably confidence. However, both ACCESS and ECMWF outperform Official at
444 23:00 and 00:00 UTC, consistent with the $\overline{\text{WPI}}$ results of Fig. 2. The NT station group results are
445 discussed in more detail in section 4.

446 At the North WA station group at 01:00, 03:00 and 04:00, Official outperforms ACCESS with
447 confidence scores of 77, 78 and 90%, respectively; Official also outperforms ECMWF at 01:00
448 and 02:00 UTC with confidence scores above 99%. Figure 9 a) shows that ECMWF's poor per-
449 formance at 01:00 and 02:00 UTC is simply due to its linear interpolation at these times, whereas
450 Official's very slight outperformance of ACCESS at 01:00, 03:00 and 04:00 is due to ACCESS's
451 climatological diurnal cycle being slightly out of phase with that of the AWS observations, and
452 the Official forecast correcting for this somewhat. Both Official and ECMWF slightly exaggerate
453 the magnitude of the climatological sea-breeze, which peaks around 09:00 UTC, with ACCESS
454 performing well in this respect.

455 At the South WA station group from 01:00 to 05:00 UTC, Official outperforms ECMWF with
456 confidence scores of at least 88%. Figure 9 b) shows that ECMWF underestimates the westerly
457 perturbations at these times, with these perturbations likely associated with boundary layer mixing
458 processes, as discussed in section a. Each of Official, ACCESS and ECMWF noticeably under-
459 estimate the amplitude of the diurnal cycle between 02:00 and 10:00 UTC, including both the
460 westerly perturbations and the southerly sea-breeze perturbations.

461 At the NSW station group from 17:00 to 19:00 UTC, Official outperforms both ACCESS and
462 ECMWF with confidence scores of at least 95% and 75%, respectively. Figure 9 c) shows
463 that these times correspond to “dimples” in the perturbation hodographs that are present in all four
464 datasets. The Official hodograph closely resembles that of ACCESS, except for this dimple, which
465 has been exaggerated relative to ACCESS. Don't know what is going on here. Figure 9 c) also

shows that although ECMWF exaggerates the amplitude of the easterly sea-breeze perturbations, it captures the narrower shape of the AWS hodograph better than Official or ACCESS.

At the SA station group from 02:00 to 05:00 UTC and 09:00 to 12:00 UTC, Official outperforms both ACCESS and ECMWF, although confidence scores do not exceed 88% and 65% respectively. Figure 9 d) shows that although the Official forecast captures the amplitude of the perturbations from 01:00 to 05:00 UTC almost perfectly, its diurnal cycle is out of phase with that of the AWS during this period, explaining why Official only slightly outperforms ACCESS in the results of Figures 8 a) and b).

For contrast, Fig. 10 presents the CWPI values and confidence scores for $CWPI_{OE}$, which represents the Official versus ECMWF comparison, for the airport stations, and airport station groups. These results show much greater similarity with the Official versus ECMWF comparisons at the coastal station groups shown in Figs. 8 c) and d), than do the analogous \overline{WPI} results in Fig. 6 and Figs. 2 c) and d). This likely because the temporal averaging has reduced the additional unpredictable variability in Official, revealing biases in Official and ECMWF that are partly shared across the three spatial scales. This point is discussed further in section 4.

Note that the hodographs in Fig. 9 are roughly elliptical in shape, suggesting that descriptive quantities can be estimated by fitting equations (5) and (6) to the zonal and meridional climatological perturbations, then calculating these quantities from the fit, as described in section 2. Figure 11 provides the R^2 values for the fits of the zonal and meridional perturbations to equations (5) and (6), respectively. The fit performs best at the coastal station group spatial scale, with R^2 generally above 95%. It also performs well at the airport station and airport station group scales, with a few exceptions, including the ACCESS and Official meridional perturbations at the Canberra airport station group, and the ECMWF zonal perturbations at Melbourne airport.

The ellipse fits are used to derive four descriptive quantities: the maximum perturbation speed, the eccentricity of the fitted ellipse, the angle the fitted ellipse's semi-major axis makes with lines of latitude, and the time maximum perturbation speed occurs. Figure 12 provides these four quantities for each dataset and location across the three spatial scales. A variety of structural differences are apparent at a number of locations and scales. For example, Fig. 12 a) shows that at Brisbane airport, the maximum AWS perturbation is at least 1 kn greater than Official, ACCESS and ECMWF, and Fig. 12 c) shows that the orientation of the AWS fitted ellipse is at least 20 degrees anti-clockwise from the other datasets. Figures 13 a) and b) show hodographs of the Brisbane airport perturbation climatology and ellipse fit, respectively. Although the ellipse fits suppress some of the asymmetric details, they capture the amplitudes and orientations of the real climatological diurnal cycles well. In this case the results show that the average AWS sea-breeze approaches from the northeast, whereas the forecast and model sea-breezes approach more from the east-northeast. To check whether this just represents a direction bias of the Brisbane Airport station, Fig. 12 shows the climatological perturbations at the nearby Spitfire Channel station (see Fig. 1 for the location of this station, and other stations referred to in this section). While the amplitude bias is smaller at Spitfire Channel than Brisbane Airport, the directional bias is at least as high. A similar directional bias is evident at the nearby Inner Beacon station (not shown), although the bias is smaller than at Spitfire Channel and Brisbane Airport. Thus, the directional bias in Official, ACCESS and ECMWF at these stations is likely genuine, and not just a consequence of biased AWS observations. Figure 1 shows there are two small islands to the east of Brisbane airport; the more northwesterly orientation of the Brisbane Airport sea-breeze suggests these islands may be redirecting winds between the east coast of Brisbane and the west coasts of these islands, and that this local effect is not being captured in Official, ACCESS or ECMWF.

Another example is the Hobart Airport station. Figure 12 c) shows that the ellipse fits for the AWS perturbations are oriented 31, 35 and 62 degrees anti-clockwise from the ECMWF, Official and ACCESS ellipse fits, respectively. Figures 11 a) and b) show that the ellipse fit for the AWS perturbations at Hobart airport only achieve R^2 values of 59% and 68% for the u and v components, respectively. However, figures 13 d) and e) show that the fit still captures orientations accurately, although it underestimates the maximum AWS perturbation. Figure 13 f) shows the climatological perturbations at the Hobart (city) station, which also show a large difference in orientation between ACCESS and AWS. Given the timing of the westerly perturbations in ACCESS, and the fact that the prevailing winds around Tasmania are westerly, these results suggest that ACCESS is exaggerating the boundary layer mixing processes involved in the diurnal cycle around Hobart.

The South WA station group also provides an interesting example. Here the ACCESS and Official ellipse fits are oriented at least 49 degrees anti-clockwise from those of AWS and ECMWF, and the ECMWF perturbations peak between 1.2 and 2.5 hours after the other datasets. These differences occur because eccentricity values are low for this station group, and Figure 9 b) shows that the westerly perturbations associated with boundary layer mixing are weaker for ECMWF than the other datasets. A similar issue affects the VIC station group, explaining why the AWS ellipse fit is oriented at least 49 degrees anti-clockwise from those of the other datasets.

The Darwin Airport, Darwin Airport station group, and NT station group provide further examples. In these cases there are timing differences between the perturbation maximums of up to 8.2 hours. Figure 14 shows that these differences occur because for some datasets, the later north to northwesterly sea-breeze perturbations dominate the diurnal wind cycle, but for other datasets the earlier easterly to southeasterly boundary layer mixing effects dominate.

4. Discussion

The results of section 3 may have some confronting implications for forecasting practice. If the goal of land-sea breeze and boundary layer mixing edits is to reduce absolute errors in the following day’s forecast of the surface wind fields, then a necessary (but not sufficient) condition for this to occur is for these edits to at least reduce the absolute errors in the diurnal component of the surface wind fields. However, the WPI comparisons in Figs. 2 and 6 suggest that this is only possible when absolute error is calculated at coarse spatial scales. If the Official forecast is based, at least partly, on an edited high resolution model guidance dataset like ACCESS, then due to the mesoscale verification issues discussed in section 1, the larger absolute errors associated with a higher resolution model completely mask the effect of the edits, with a lower resolution unedited model like ECMWF scoring better overall. While the CWPI results in Figs. 8 and 6 suggest that forecaster edits can improve the accuracy of diurnal wind cycles in a climatological sense, it is not clear if these improvements have operational significance.

To investigate these ideas further, consider first just the zonal components of the AWS and Official wind perturbations, denoted by u_{AWS} and u_{O} respectively. Considering just the values at a particular hour UTC, at a particular station, over the entire June, July, August time period, the mean square error $\text{mse}(u_{\text{AWS}}, u_{\text{O}}) = \overline{(u_{\text{AWS}} - u_{\text{O}})^2}$ can be decomposed

$$\text{mse}(u_{\text{AWS}}, u_{\text{O}}) = \underbrace{\text{var}(u_{\text{AWS}}) + \text{var}(u_{\text{O}}) - 2 \cdot \text{covar}(u_{\text{AWS}}, u_{\text{O}})}_{\text{var}(u_{\text{AWS}} - u_{\text{O}})} + \underbrace{(\bar{u}_{\text{AWS}} - \bar{u}_{\text{O}})^2}_{\text{squared bias}} \quad (8)$$

where var, covar and over-bars denote the sample variance, covariance and mean respectively. The first three terms are the total variance of $u_{\text{AWS}} - u_{\text{O}}$, whereas the last term is the square of the bias between u_{AWS} and u_{O} . Note that the mean square error $\text{mse}(u_{\text{AWS}}, u_{\text{O}})$ is closely related to $\overline{\text{WPI}}$, which is the difference between the mean absolute error of Official and AWS, and a model guidance dataset and AWS. Similarly, the CWPI is closely related to the squared bias component

556 $(\bar{u}_{AWS} - \bar{u}_O)^2$ of the mean square error. Equation (8) can also be applied to wind perturbations that
 557 have first been spatially averaged over a station group, and to $mse(u_{AWS}, u_E)$ and $mse(u_{AWS}, u_A)$,
 558 where u_E and u_A are the ECMWF and ACCESS zonal perturbations, respectively.

559 Figure 15 shows each term in the mean square error decomposition of equation 8 for both
 560 $mse(u_{AWS}, u_O)$ and $mse(u_{AWS}, u_E)$, for Darwin Airport, the Darwin station group, and the NT
 561 station group. This region provides an interesting case study because Fig. 6 shows that Offi-
 562 cial has some skill at both Darwin Airport and over Darwin Airport station groups, in contrast
 563 to most other locations. At Darwin Airport, $mse(u_{AWS}, u_O)$ exceeds $mse(u_{AWS}, u_E)$ from 04:00
 564 to 16:00 UTC due to higher total variance, whereas outside of these times $mse(u_{AWS}, u_E)$ ex-
 565 ceeds $mse(u_{AWS}, u_O)$ due to larger bias. The higher total variance of $u_{AWS} - u_O$ occurs because
 566 $var(u_O) > var(u_E)$. This additional variability is mostly random from 04:00 to 14:00 UTC, i.e. u_O
 567 is not sufficiently correlated with u_{AWS} at these times for the additional variability of u_O to pro-
 568 duce a reduction in mean square error. Thus, while the bias between Official and AWS is lower,
 569 or about the same, as that between ECMWF and AWS, the higher random variability of Official
 570 results in higher mean square error for most of the day. Figure 16 shows similar conclusions can be
 571 drawn for the meridional perturbations at Darwin Airport, although in this case $var(u_O) > var(u_E)$
 572 for the entire day. Most of the difference between the WPI and CWPI scores for the Official ver-
 573 sus ECMWF comparison at Darwin Airport in Figures 6 and 10, respectively, can be explained
 574 through the different mean square error and bias terms for the zonal perturbations alone.

575 Figure 14 a) shows that ECMWF's climatological perturbations at Darwin Airport underestimate
 576 the easterly perturbations from 00:00 to 03:00 UTC, which are presumably associated with bound-
 577 ary layer mixing processes. Official does a better job of resolving these easterly perturbations, but
 578 is generally outperformed by ECMWF in resolving the northerly sea-breeze perturbations. Similar
 579 points can be made for the Darwin and NT coastal station groups. While spatial averaging reduces

580 a portion of the unpredictable variability in Official, Official also often has larger meridional biases
581 at these scales compared to ECMWF. Figures 14 and 12 show that these biases can be explained
582 in terms of amplitude and orientation differences between Official, ECMWF and AWS. Figures
583 analogous to Figs. 15 and 16, but for other locations around Australia, show similar results, but
584 without the large meridional biases present in the Official forecast at the Darwin Airport station
585 group and NT coastal station group.

586 These examples illustrate the idea that the additional unpredictable variability introduced by a
587 higher resolution edited forecast needs to be “paid for” by a reduction in bias, otherwise the net re-
588 sult will just be an increase in error. However, although a high resolution edited forecast may have
589 higher mean squared error compared with observations than an unedited low resolution model,
590 the former may capture variability more realistically, and hence better represent the possibility of
591 extremes, even if the timing of these extremes is unpredictable; which of the two constitutes a
592 better forecast therefore depends entirely on the application. For instance, in engineering applica-
593 tions, the possibility of wind extremes of a certain magnitude may be most important, regardless
594 of when they occur, whereas in aviation or sailing it may be more important to minimise the mean
595 square error. The fact that high and low resolution model guidance products are used at different
596 times, and on different days, implies that the Official forecast is inconsistent in which measures of
597 accuracy it intends to maximise, and more thought therefore needs to be given to this issue.

598 **5. Conclusion**

599 We have

References

- Abkar, M., A. Sharifi, and F. Porté-Agel, 2016: Wake flow in a wind farm during a diurnal cycle. *Journal of Turbulence*, **17** (4), 420–441, doi:10.1080/14685248.2015.1127379, URL <https://doi.org/10.1080/14685248.2015.1127379>, <https://doi.org/10.1080/14685248.2015.1127379>.
- Brown, A. L., C. L. Vincent, T. P. Lane, E. Short, and H. Nguyen, 2017: Scatterometer estimates of the tropical sea-breeze circulation near Darwin, with comparison to regional models. *Quart. J. Roy. Meteor. Soc.*, doi:10.1002/qj.3131.
- Bureau of Meteorology, 2010: Operational implementation of the ACCESS numerical weather prediction systems. Tech. rep., Bureau of Meteorology, Melbourne, Victoria. [Available online at <http://www.bom.gov.au/australia/charts/bulletins/apob83.pdf>].
- Bureau of Meteorology, 2019: Meteye. Bureau of Meteorology, [Available online at <http://www.bom.gov.au/australia/meteye/>].
- Dai, A., and C. Deser, 1999: Diurnal and semidiurnal variations in global surface wind and divergence fields. *Journal of Geophysical Research*, **104**, 31 109–31 125.
- Ebert, E., and J. McBride, 2000: Verification of precipitation in weather systems: determination of systematic errors. *Journal of Hydrology*, **239** (1), 179 – 202, doi:[https://doi.org/10.1016/S0022-1694\(00\)00343-7](https://doi.org/10.1016/S0022-1694(00)00343-7), URL <http://www.sciencedirect.com/science/article/pii/S0022169400003437>.
- Ebert, E. E., 2008: Fuzzy verification of high-resolution gridded forecasts: a review and proposed framework. *Meteor. Appl.*, **15** (1), 51–64, doi:10.1002/met.25, URL <https://rmets.onlinelibrary.wiley.com/doi/abs/10.1002/met.25>, <https://rmets.onlinelibrary.wiley.com/doi/pdf/10.1002/met.25>.

- 622 Efron, B., 1979: Bootstrap methods: Another look at the jackknife. *The Annals of Statistics*, **7** (1),
623 1–26, doi:10.1214/aos/1176344552.
- 624 Englberger, A., and A. Dörnbrack, 2018: Impact of the diurnal cycle of the atmospheric
625 boundary layer on wind-turbine wakes: A numerical modelling study. *Boundary-Layer Me-*
626 *teorology*, **166** (3), 423–448, doi:10.1007/s10546-017-0309-3, URL [https://doi.org/10.1007/](https://doi.org/10.1007/s10546-017-0309-3)
627 [s10546-017-0309-3](https://doi.org/10.1007/s10546-017-0309-3).
- 628 European Center for Medium Range Weather Forecasting, 2018: *Part IV : Physical processes*.
629 No. 4, IFS Documentation, European Center for Medium Range Weather Forecasting, [Avail-
630 able online at <https://www.ecmwf.int/node/18714>].
- 631 Gille, S. T., S. G. Llewellyn Smith, and N. M. Statom, 2005: Global observations of the
632 land breeze. *Geophysical Research Letters*, **32** (5), doi:10.1029/2004GL022139, URL [https://](https://agupubs.onlinelibrary.wiley.com/doi/abs/10.1029/2004GL022139)
633 agupubs.onlinelibrary.wiley.com/doi/abs/10.1029/2004GL022139.
- 634 Griffiths, D., H. Jack, M. Foley, I. Ioannou, and M. Liu, 2017: Advice for automation of forecasts:
635 a framework. Tech. rep., Bureau of Meteorology, Melbourne, Victoria. [Available online at
636 <http://www.bom.gov.au/research/publications/researchreports/BRR-021.pdf>].
- 637 Haurwitz, B., 1947: Comments on the sea-breeze circulation. *Journal of Meteorol-*
638 *ogy*, **4** (1), 1–8, doi:10.1175/1520-0469(1947)004<0001:COTSBC>2.0.CO;2, URL
639 [https://doi.org/10.1175/1520-0469\(1947\)004<0001:COTSBC>2.0.CO;2](https://doi.org/10.1175/1520-0469(1947)004<0001:COTSBC>2.0.CO;2),
640 [https://doi.org/10.1175/1520-0469\(1947\)004<0001:COTSBC>2.0.CO;2](https://doi.org/10.1175/1520-0469(1947)004<0001:COTSBC>2.0.CO;2).
- 641 Hoxit, L. R., 1975: Diurnal variations in planetary boundary-layer winds over land. *Boundary-*
642 *Layer Meteorology*, **8** (1), 21–38, doi:10.1007/BF02579391, URL [https://doi.org/10.1007/](https://doi.org/10.1007/BF02579391)
643 [BF02579391](https://doi.org/10.1007/BF02579391).

644 Kusuda, M., and P. Alpert, 1983: Anti-clockwise rotation of the wind hodograph.
 645 part i: Theoretical study. *Journal of the Atmospheric Sciences*, **40** (2), 487–499,
 646 doi:10.1175/1520-0469(1983)040<0487:ACROTW>2.0.CO;2, URL [https://doi.org/10.1175/](https://doi.org/10.1175/1520-0469(1983)040<0487:ACROTW>2.0.CO;2)
 647 1520-0469(1983)040<0487:ACROTW>2.0.CO;2.

648 Lee, X., 2018: *Fundamentals of boundary-layer meteorology*. Springer atmospheric sciences,
 649 Springer.

650 Lock, A. P., A. R. Brown, M. R. Bush, G. M. Martin, and R. N. B. Smith, 2000: A new bound-
 651 ary layer mixing scheme. part i: Scheme description and single-column model tests. *Monthly*
 652 *Weather Review*, **128** (9), 3187–3199, doi:10.1175/1520-0493(2000)128<3187:ANBLMS>2.
 653 0.CO;2, URL [https://doi.org/10.1175/1520-0493\(2000\)128<3187:ANBLMS>2.0.CO;2](https://doi.org/10.1175/1520-0493(2000)128<3187:ANBLMS>2.0.CO;2), [https://doi.org/10.1175/1520-0493\(2000\)128<3187:ANBLMS>2.0.CO;2](https://doi.org/10.1175/1520-0493(2000)128<3187:ANBLMS>2.0.CO;2).

655 Louis, J.-F., 1979: A parametric model of vertical eddy fluxes in the atmosphere. *Boundary-*
 656 *Layer Meteorology*, **17** (2), 187–202, doi:10.1007/BF00117978, URL [https://doi.org/10.1007/](https://doi.org/10.1007/BF00117978)
 657 BF00117978.

658 Lynch, K. J., D. J. Brayshaw, and A. Charlton-Perez, 2014: Verification of european sub-
 659 seasonal wind speed forecasts. *Monthly Weather Review*, **142** (8), 2978–2990, doi:10.1175/
 660 MWR-D-13-00341.1, URL <https://doi.org/10.1175/MWR-D-13-00341.1>, [https://doi.org/10.](https://doi.org/10.1175/MWR-D-13-00341.1)
 661 1175/MWR-D-13-00341.1.

662 Mass, C. F., D. Ovens, K. Westrick, and B. A. Colle, 2002: Does increasing horizon-
 663 tal resolution produce more skillful forecasts? *Bulletin of the American Meteorologi-*
 664 *cal Society*, **83** (3), 407–430, doi:10.1175/1520-0477(2002)083<0407:DIHRPM>2.3.CO;2,
 665 URL [https://doi.org/10.1175/1520-0477\(2002\)083<0407:DIHRPM>2.3.CO;2](https://doi.org/10.1175/1520-0477(2002)083<0407:DIHRPM>2.3.CO;2), [https://doi.org/](https://doi.org/10.1175/1520-0477(2002)083<0407:DIHRPM>2.3.CO;2)
 666 10.1175/1520-0477(2002)083<0407:DIHRPM>2.3.CO;2.

667 Miller, S. T. K., B. D. Keim, R. W. Talbot, and H. Mao, 2003: Sea breeze: Structure, forecasting,
 668 and impacts. *Reviews of Geophysics*, **41** (3), doi:10.1029/2003RG000124, URL [https://doi.org/](https://doi.org/10.1029/2003RG000124)
 669 10.1029/2003RG000124.

670 Murphy, A. H., 1991: Forecast verification: Its complexity and dimensionality. *Monthly*
 671 *Weather Review*, **119** (7), 1590–1601, doi:10.1175/1520-0493(1991)119<1590:FVICAD>2.0.
 672 CO;2, URL [https://doi.org/10.1175/1520-0493\(1991\)119<1590:FVICAD>2.0.CO;2](https://doi.org/10.1175/1520-0493(1991)119<1590:FVICAD>2.0.CO;2), [https://doi.](https://doi.org/10.1175/1520-0493(1991)119<1590:FVICAD>2.0.CO;2)
 673 [org/10.1175/1520-0493\(1991\)119<1590:FVICAD>2.0.CO;2](https://doi.org/10.1175/1520-0493(1991)119<1590:FVICAD>2.0.CO;2).

674 Physick, W. L., and D. J. Abbs, 1992: Flow and plume dispersion in a coastal valley. *Journal*
 675 *of Applied Meteorology*, **31** (1), 64–73, doi:10.1175/1520-0450(1992)031<0064:FAPDIA>2.0.
 676 CO;2, URL [https://doi.org/10.1175/1520-0450\(1992\)031<0064:FAPDIA>2.0.CO;2](https://doi.org/10.1175/1520-0450(1992)031<0064:FAPDIA>2.0.CO;2), [https://doi.](https://doi.org/10.1175/1520-0450(1992)031<0064:FAPDIA>2.0.CO;2)
 677 [org/10.1175/1520-0450\(1992\)031<0064:FAPDIA>2.0.CO;2](https://doi.org/10.1175/1520-0450(1992)031<0064:FAPDIA>2.0.CO;2).

678 Pinson, P., and R. Hagedorn, 2012: Verification of the ecmwf ensemble forecasts of wind
 679 speed against analyses and observations. *Meteor. Appl.*, **19** (4), 484–500, doi:10.1002/
 680 met.283, URL <https://rmets.onlinelibrary.wiley.com/doi/abs/10.1002/met.283>, [https://rmets.](https://rmets.onlinelibrary.wiley.com/doi/pdf/10.1002/met.283)
 681 [onlinelibrary.wiley.com/doi/pdf/10.1002/met.283](https://rmets.onlinelibrary.wiley.com/doi/pdf/10.1002/met.283).

682 Rife, D. L., and C. A. Davis, 2005: Verification of temporal variations in mesoscale numeri-
 683 cal wind forecasts. *Monthly Weather Review*, **133** (11), 3368–3381, doi:10.1175/MWR3052.1,
 684 URL <https://doi.org/10.1175/MWR3052.1>, <https://doi.org/10.1175/MWR3052.1>.

685 SciPy, 2019: Optimization and root finding (scipy.optimize). SciPy, [Available online at <https://docs.scipy.org/doc/scipy/reference/optimize.html>].
 686 <https://docs.scipy.org/doc/scipy/reference/optimize.html>].

687 Svensson, G., and Coauthors, 2011: Evaluation of the diurnal cycle in the atmospheric boundary
 688 layer over land as represented by a variety of single-column models: The second gabl's experi-

ment. *Boundary-Layer Meteorology*, **140** (2), 177–206, doi:10.1007/s10546-011-9611-7, URL
<https://doi.org/10.1007/s10546-011-9611-7>.

Vincent, C. L., and T. P. Lane, 2016: Evolution of the diurnal precipitation cycle with the passage of a madden–julian oscillation event through the maritime continent. *Monthly Weather Review*, **144** (5), 1983–2005, doi:10.1175/MWR-D-15-0326.1, URL <https://doi.org/10.1175/MWR-D-15-0326.1>, <https://doi.org/10.1175/MWR-D-15-0326.1>.

Wilks, D. S., 2011: *Statistical methods in the atmospheric sciences. [electronic resource]*. International geophysics series: v. 100, Elsevier.

Zaron, E. D., and G. D. Egbert, 2006: Estimating open-ocean barotropic tidal dissipation: The hawaiian ridge. *Journal of Physical Oceanography*, **36** (6), 1019–1035, doi:10.1175/JPO2878.1, URL <https://doi.org/10.1175/JPO2878.1>, <https://doi.org/10.1175/JPO2878.1>.

Zwiers, F. W., and H. von Storch, 1995: Taking serial correlation into account in tests of the mean. *Journal of Climate*, **8** (2), 336–351, doi:10.1175/1520-0442(1995)008<0336:TSCIAI>2.0.CO;2, URL [https://doi.org/10.1175/1520-0442\(1995\)008<0336:TSCIAI>2.0.CO;2](https://doi.org/10.1175/1520-0442(1995)008<0336:TSCIAI>2.0.CO;2), [https://doi.org/10.1175/1520-0442\(1995\)008<0336:TSCIAI>2.0.CO;2](https://doi.org/10.1175/1520-0442(1995)008<0336:TSCIAI>2.0.CO;2).

704 **LIST OF TABLES**

705	Table 1.	Average 10 m wind speeds for austral winter (June, July August) 2018, and	
706		austral summer (December, January, February) 2017/18 across the eight Aus-	
707		tralian capital city airport weather stations.	34

Airport	Austral Summer	Austral Winter
Darwin	6.3 kn	6.2 kn
Brisbane	8.6 kn	7.0 kn
Perth	11.3 kn	7.9 kn
Sydney	12.2 kn	10.2 kn
Adelaide	9.5 kn	10.3 kn
Canberra	7.4 kn	7.9 kn
Melbourne	10.0 kn	12.1 kn
Hobart	10.0 kn	8.7 kn

708 TABLE 1. Average 10 m wind speeds for austral winter (June, July August) 2018, and austral summer (De-
709 cember, January, February) 2017/18 across the eight Australian capital city airport weather stations.

710	LIST OF FIGURES	
711	Fig. 1. Locations of the automatic weather stations used in this study. Stars indicate capital city	
712	airport stations. Height and depth shading intervals every 200 and 1000 m, respectively.	37
713	Fig. 2. Heatmaps of \overline{WPI} values and confidence scores for each coastal station group and hour of	
714	the day: a) and b), Official versus ACCESS, c) and d) Official versus ECMWF, e) and f)	
715	ECMWF versus ACCESS. Positive \overline{WPI} values mean that the former dataset in each pair	
716	is on average closer to observations than the latter dataset. Confidence scores provide the	
717	probability the population \overline{WPI} is greater than zero. Values within the heatmaps are accurate	
718	to two significant figures.	38
719	Fig. 3. Time series, a) and b), of \overline{WPI}_{OA} and \overline{WPI}_{OE} for, a), the NT station group at 23:00 UTC,	
720	and b), the south WA station group at 05:00 UTC. Hodographs, c) to f), showing change in	
721	winds, c) and e), and wind perturbations, d) and f), for the NT station group, c) and d), and	
722	south WA station group, e) and f).	39
723	Fig. 4. Time series, a) and b), of \overline{WPI}_{OA} and \overline{WPI}_{OE} for, a), the NT station group at 23:00 UTC,	
724	and b), the south WA station group at 05:00 UTC. Hodographs, c) to f), showing change in	
725	winds, c) and e), and wind perturbations, d) and f), for the NT station group, c) and d), and	
726	south WA station group, e) and f).	40
727	Fig. 5. Hodographs showing change in winds with height at, a), Darwin Airport, and b), Perth	
728	Airport.	41
729	Fig. 6. The \overline{WPI}_{OE} (Official versus ECMWF comparison) values, a) and c), and confidence scores,	
730	b) and d), for the airport stations, a) and b), and airport station groups, c) and d), respectively.	42
731	Fig. 7. As in Fig. 6, but for the \overline{WPI}_{EA} (ECMWF versus ACCESS comparison) values and confi-	
732	dence scores.	43
733	Fig. 8. As in Fig. 2, but for the CWPI values and confidence scores.	44
734	Fig. 9. Climatological hodographs.	45
735	Fig. 10. As in Fig. 6, but for the cwpi values and confidence scores.	46
736	Fig. 11. Could also provide an analogous figure showing the use of the function α provides a signifi-	
737	cant improvement over the basic ellipse fit - or instead just quote some numbers? Or maybe	
738	these figures are entirely unnecessary?	47
739	Fig. 12. Ellipse fits. If we were to include any analysis for alternative time periods (e.g. summer	
740	2017/18 for contrast; or could do 18/19 if I were to go back to BoM to get the data) a copy	
741	of this figure could be a good choice. Could explain changes in diurnal cycle properties, e.g.	
742	amplitude, with seasonal changes to background winds, heating, etc. Note some issues with	
743	timing and amplitude values due to asymmetry - could instead just show eccentricity and	
744	orientation values?	48
745	Fig. 13. Ellipse fits. Could instead just provide one example.	49
746	Fig. 14. Ellipse fits. Could also include the ellipses, but this makes the figure very large.	50

747	Fig. 15. Actual perturbation standard deviation values. Note that official performs the worst at this	
748	scale!	51
749	Fig. 16. Actual perturbation standard deviation values. Note that official performs the worst at this	
750	scale!	52

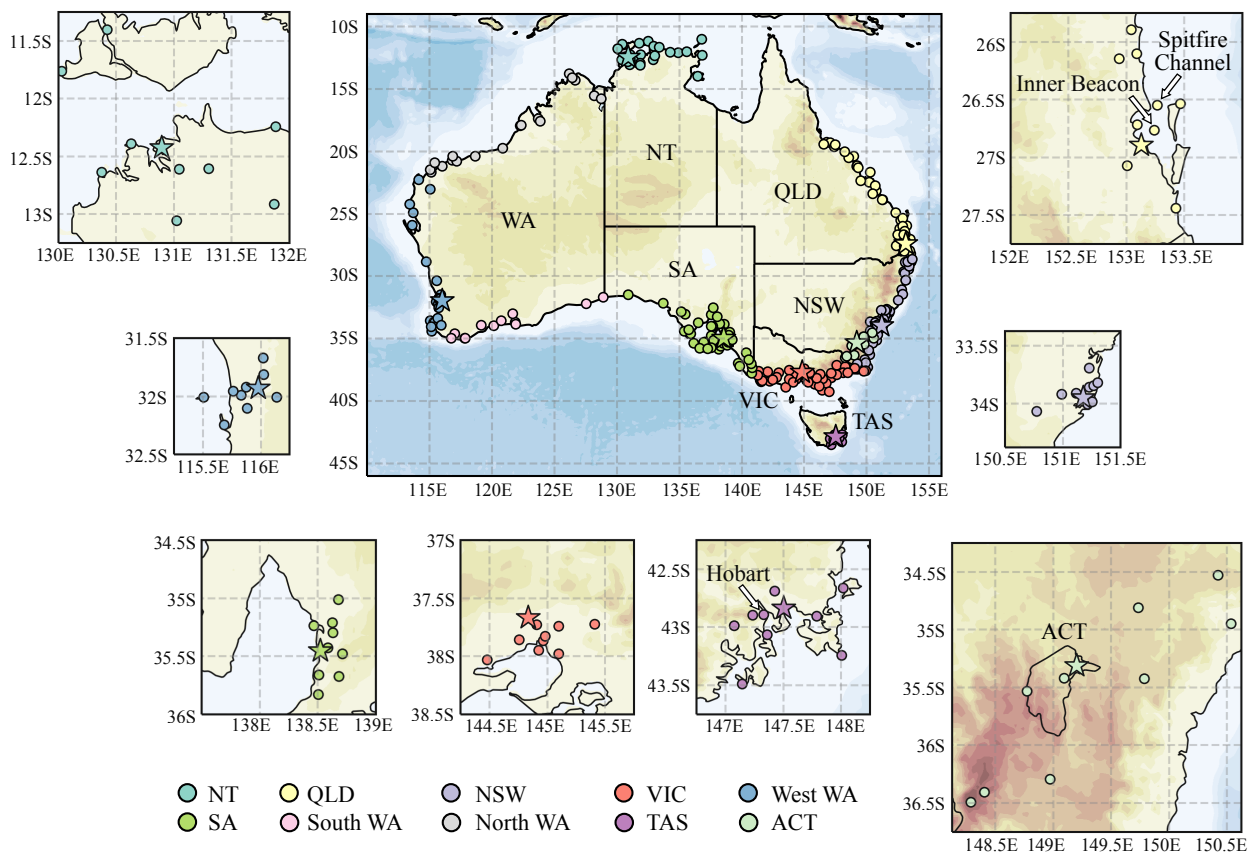


FIG. 1. Locations of the automatic weather stations used in this study. Stars indicate capital city airport stations. Height and depth shading intervals every 200 and 1000 m, respectively.

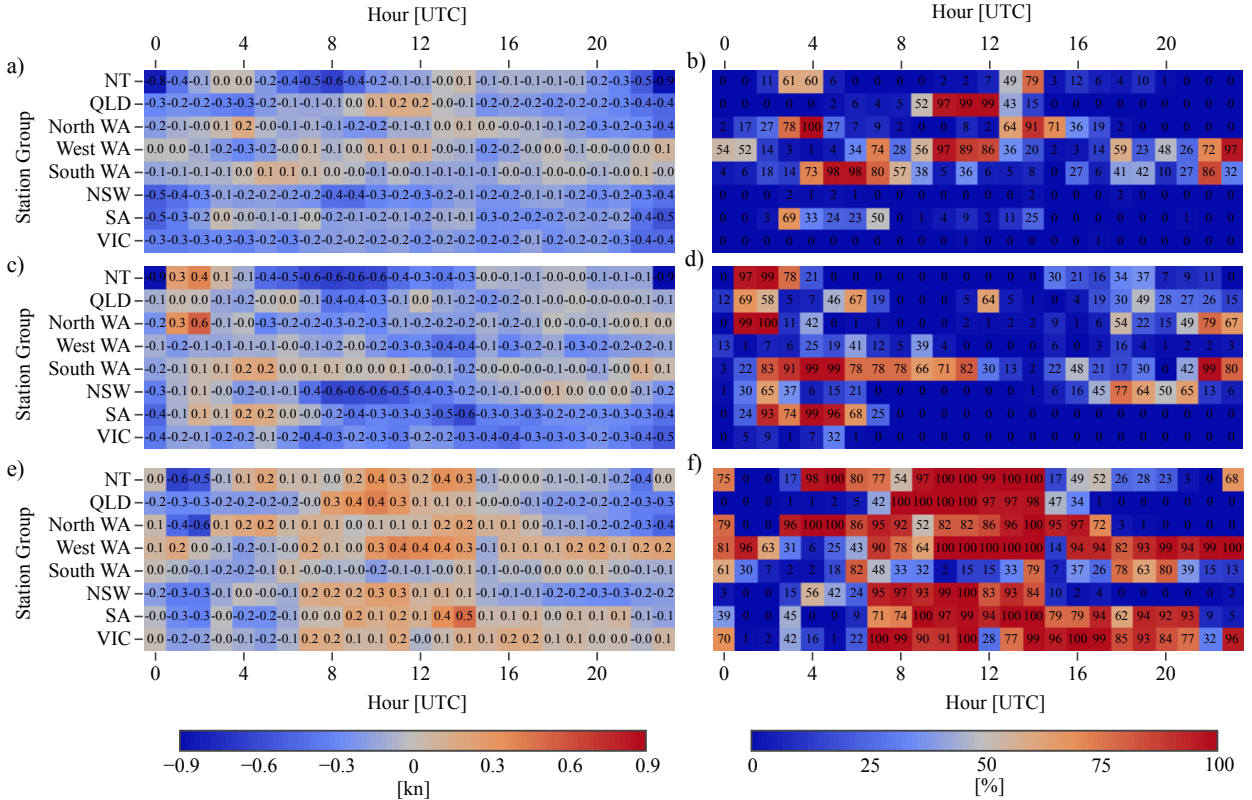


FIG. 2. Heatmaps of $\overline{\text{WPI}}$ values and confidence scores for each coastal station group and hour of the day: a) and b), Official versus ACCESS, c) and d) Official versus ECMWF, e) and f) ECMWF versus ACCESS. Positive $\overline{\text{WPI}}$ values mean that the former dataset in each pair is on average closer to observations than the latter dataset. Confidence scores provide the probability the population $\overline{\text{WPI}}$ is greater than zero. Values within the heatmaps are accurate to two significant figures.

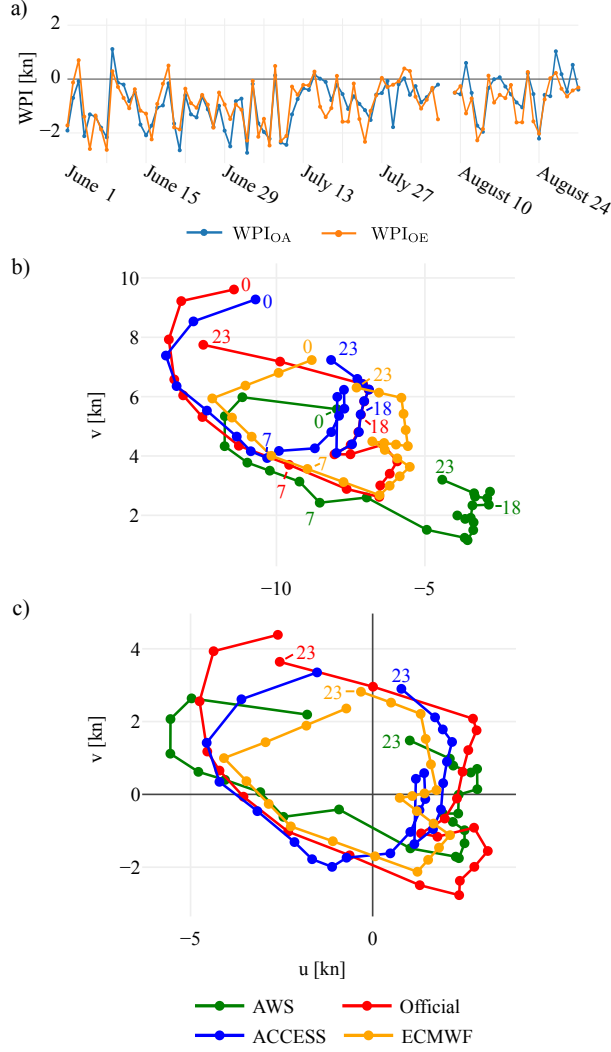


FIG. 3. Time series, a) and b), of \overline{WPI}_{OA} and \overline{WPI}_{OE} for, a), the NT station group at 23:00 UTC, and b), the south WA station group at 05:00 UTC. Hodographs, c) to f), showing change in winds, c) and e), and wind perturbations, d) and f), for the NT station group, c) and d), and south WA station group, e) and f).

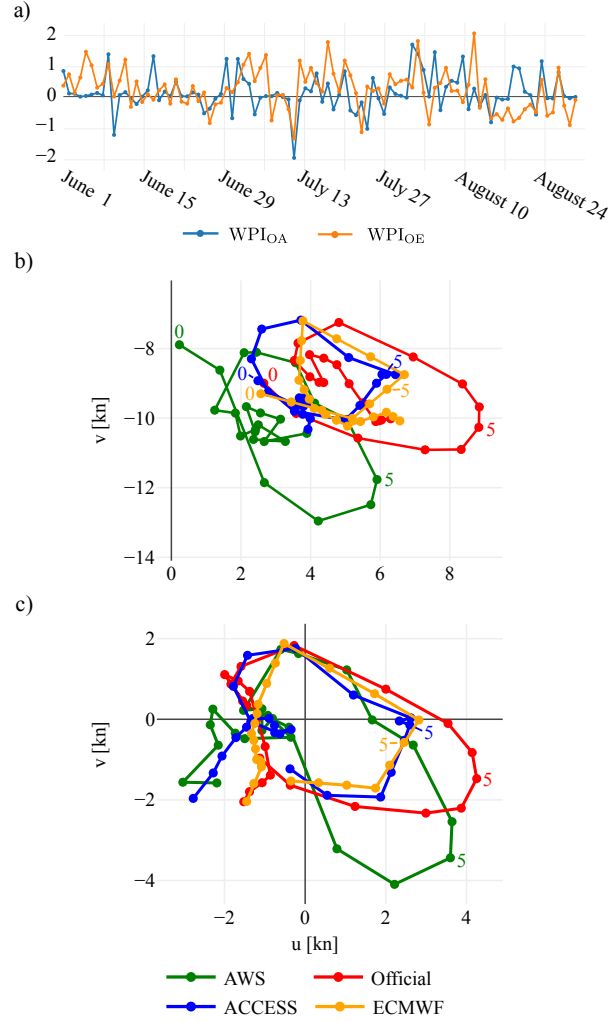


FIG. 4. Time series, a) and b), of \overline{WPI}_{OA} and \overline{WPI}_{OE} for, a), the NT station group at 23:00 UTC, and b), the south WA station group at 05:00 UTC. Hodographs, c) to f), showing change in winds, c) and e), and wind perturbations, d) and f), for the NT station group, c) and d), and south WA station group, e) and f).

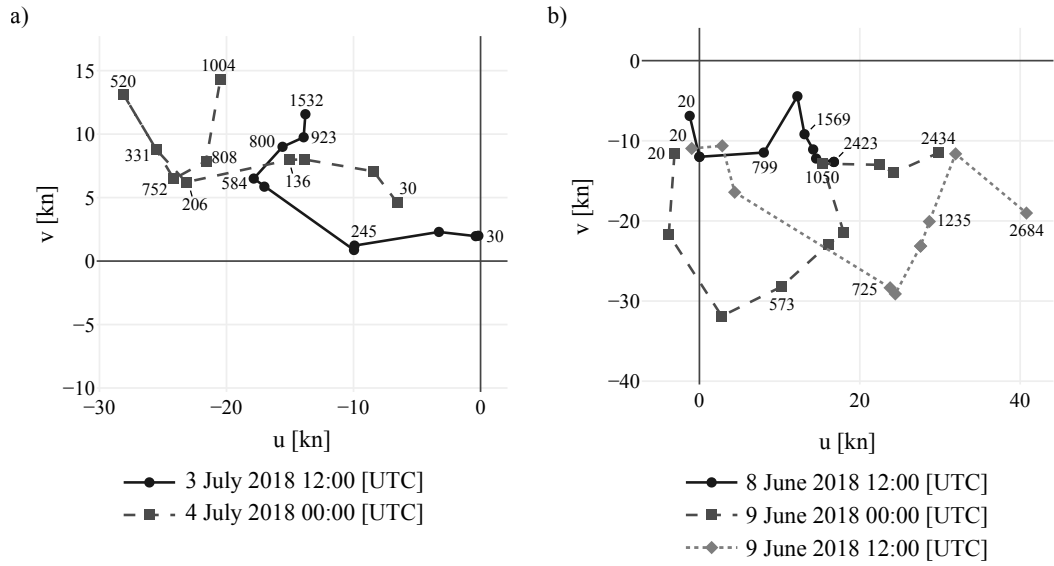


FIG. 5. Hodographs showing change in winds with height at, a), Darwin Airport, and b), Perth Airport.

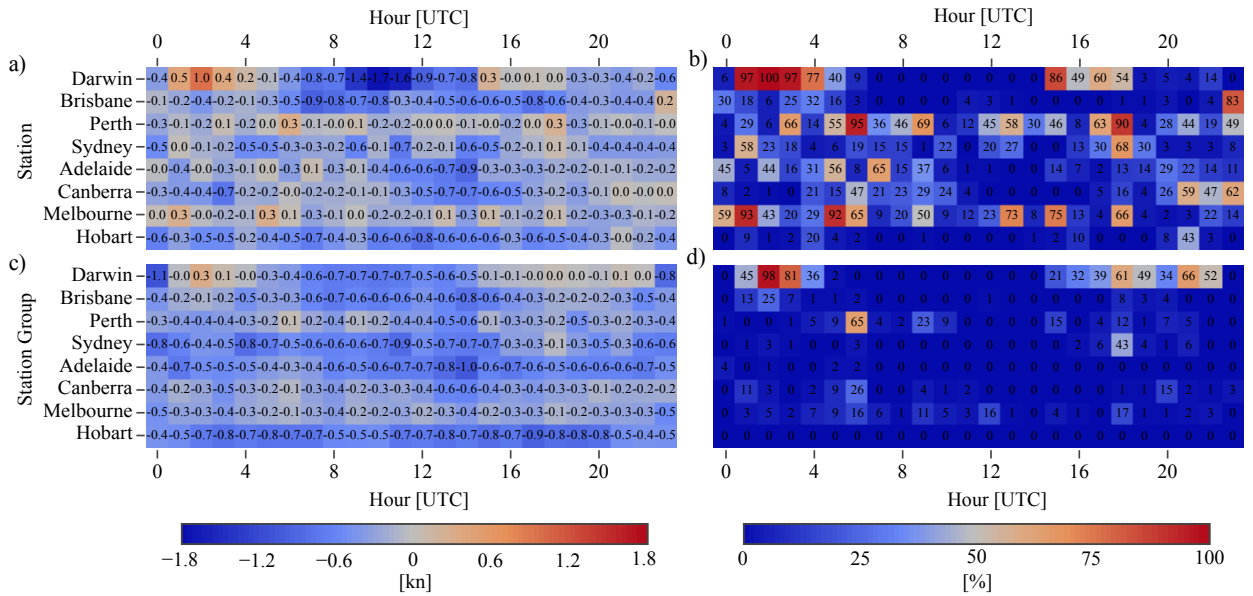


FIG. 6. The \overline{WPI}_{OE} (Official versus ECMWF comparison) values, a) and c), and confidence scores, b) and d), for the airport stations, a) and b), and airport station groups, c) and d), respectively.

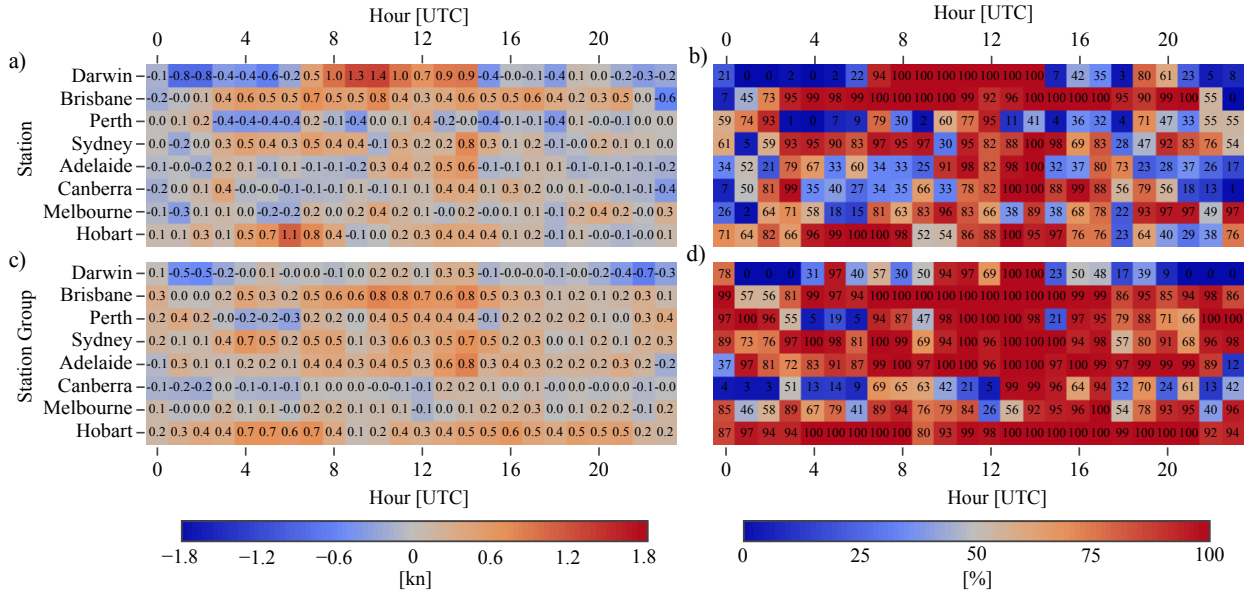


FIG. 7. As in Fig. 6, but for the $\overline{\text{WPI}}_{\text{EA}}$ (ECMWF versus ACCESS comparison) values and confidence scores.

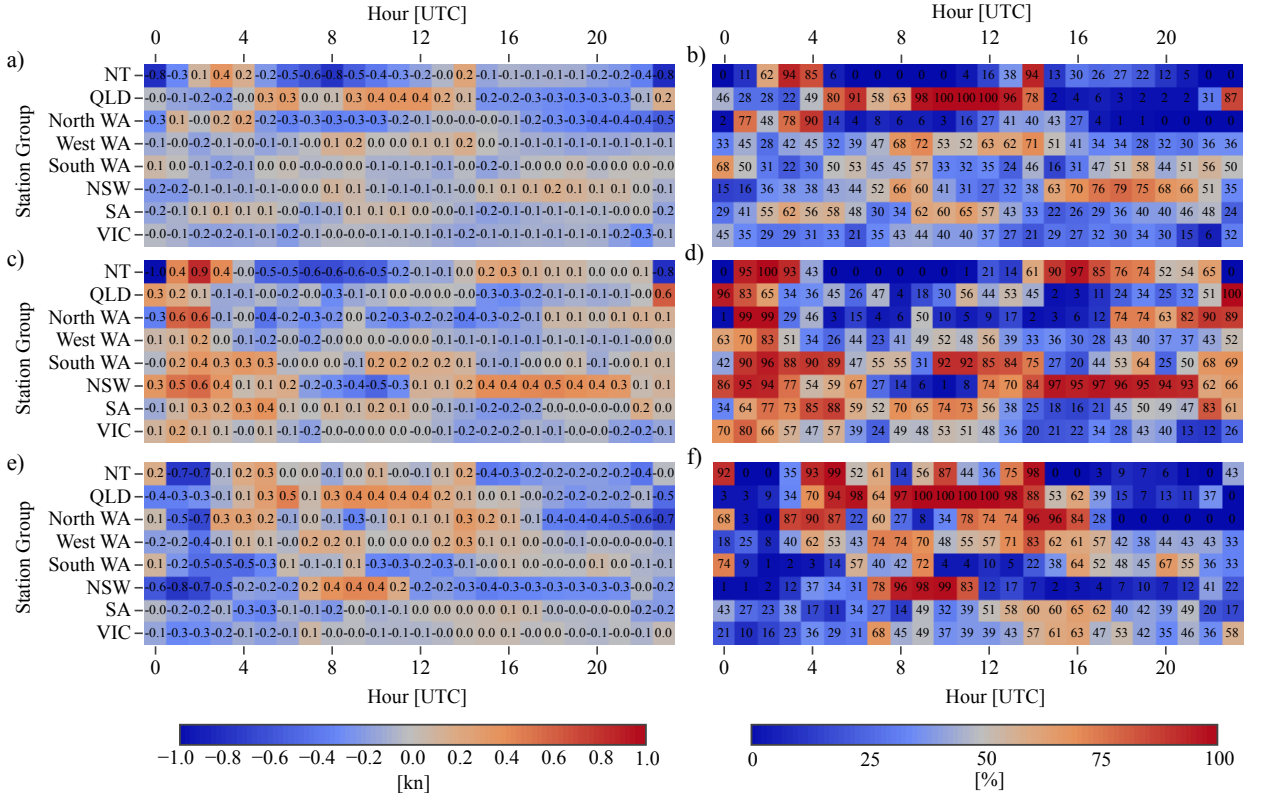


FIG. 8. As in Fig. 2, but for the CWPI values and confidence scores.

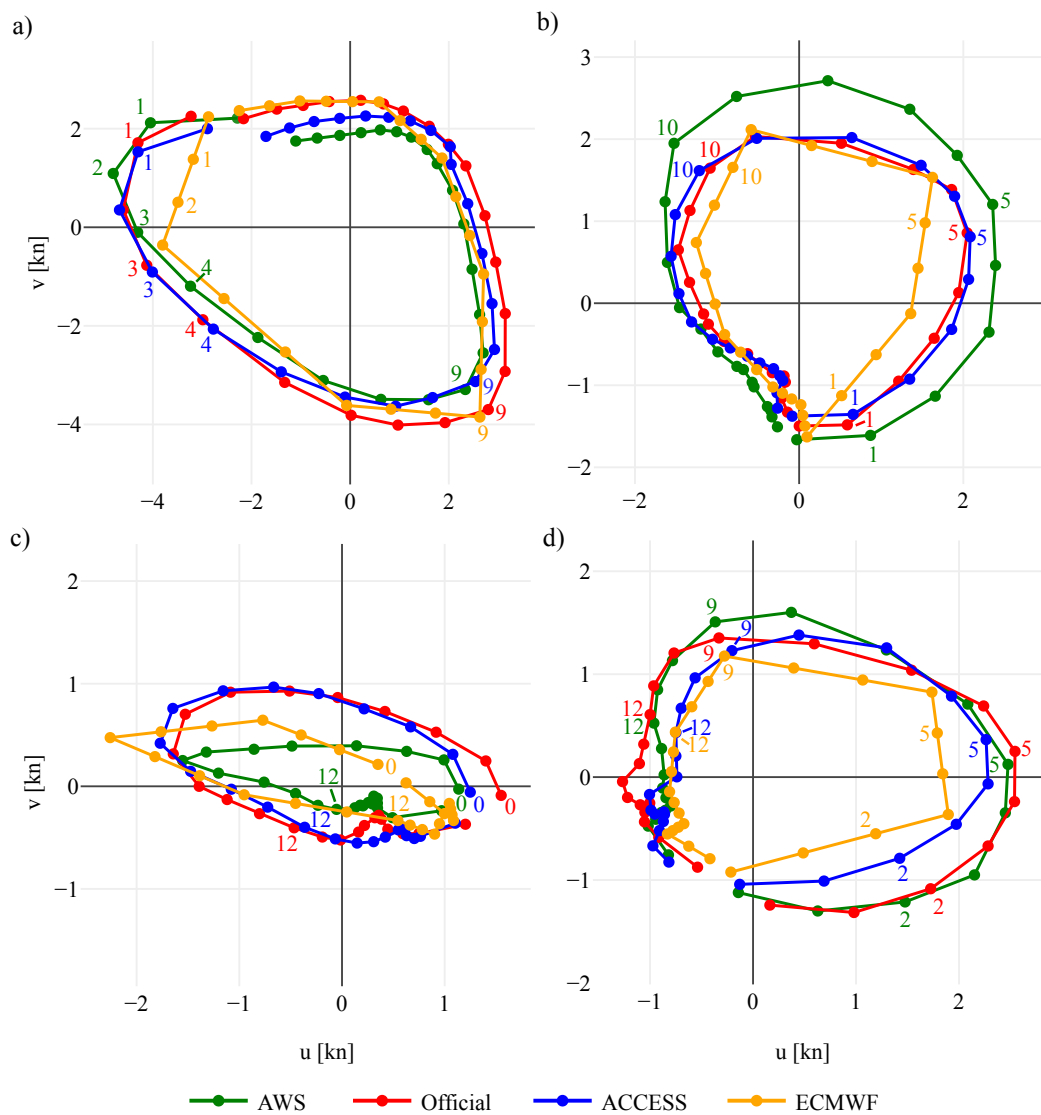


FIG. 9. Climatological hodographs.

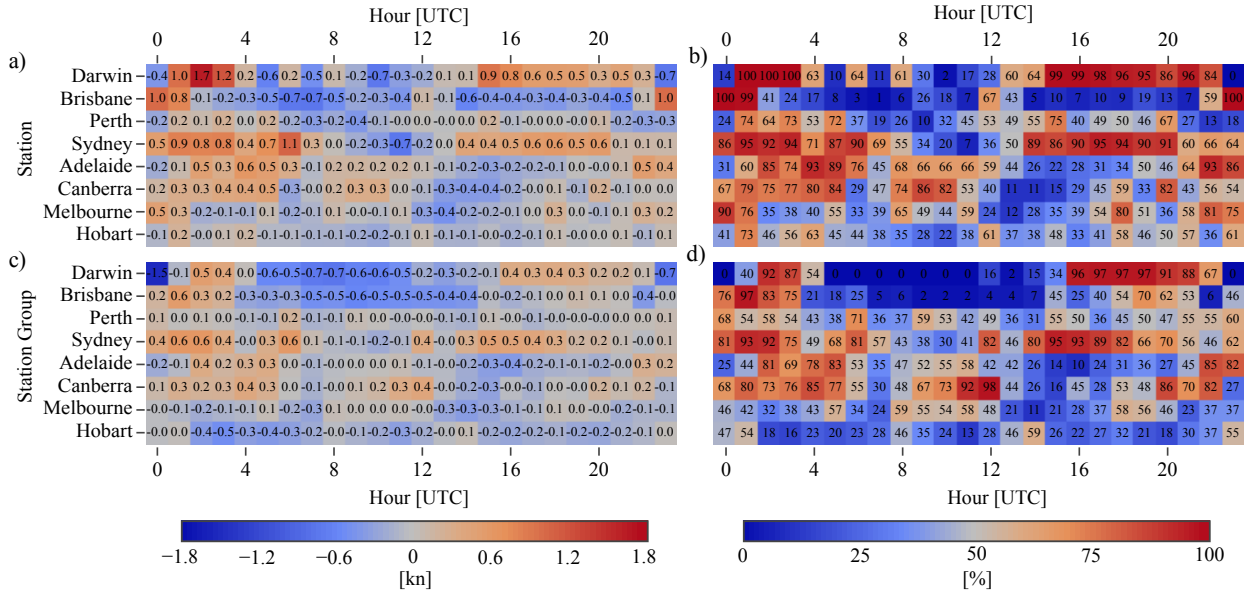


FIG. 10. As in Fig. 6, but for the cwpi values and confidence scores.

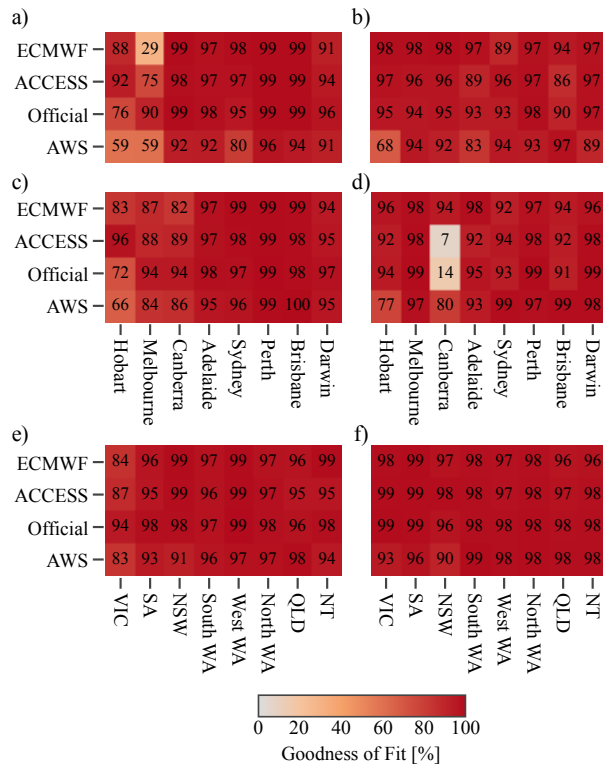


FIG. 11. Could also provide an analogous figure showing the use of the function α provides a significant improvement over the basic ellipse fit - or instead just quote some numbers? Or maybe these figures are entirely unnecessary?

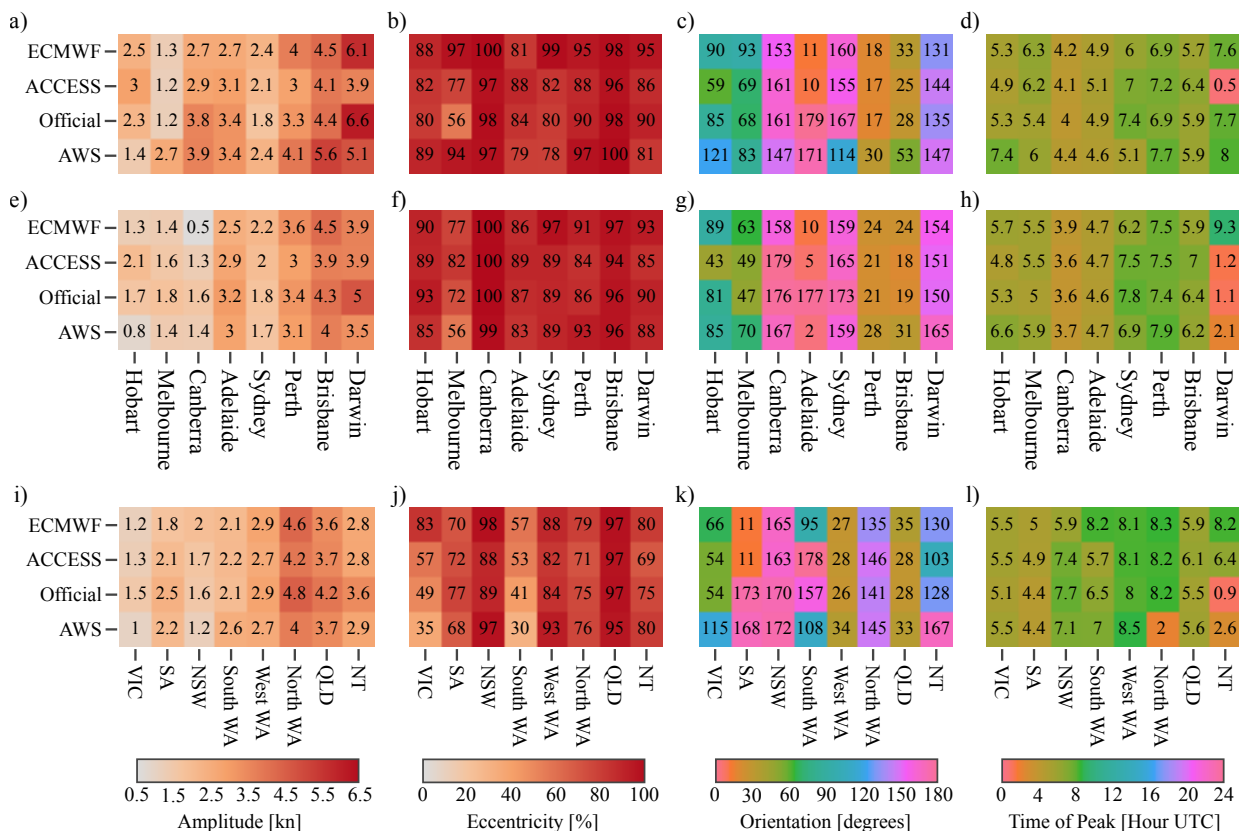


FIG. 12. Ellipse fits. If we were to include any analysis for alternative time periods (e.g. summer 2017/18 for contrast; or could do 18/19 if I were to go back to BoM to get the data) a copy of this figure could be a good choice. Could explain changes in diurnal cycle properties, e.g. amplitude, with seasonal changes to background winds, heating, etc. Note some issues with timing and amplitude values due to asymmetry - could instead just show eccentricity and orientation values?

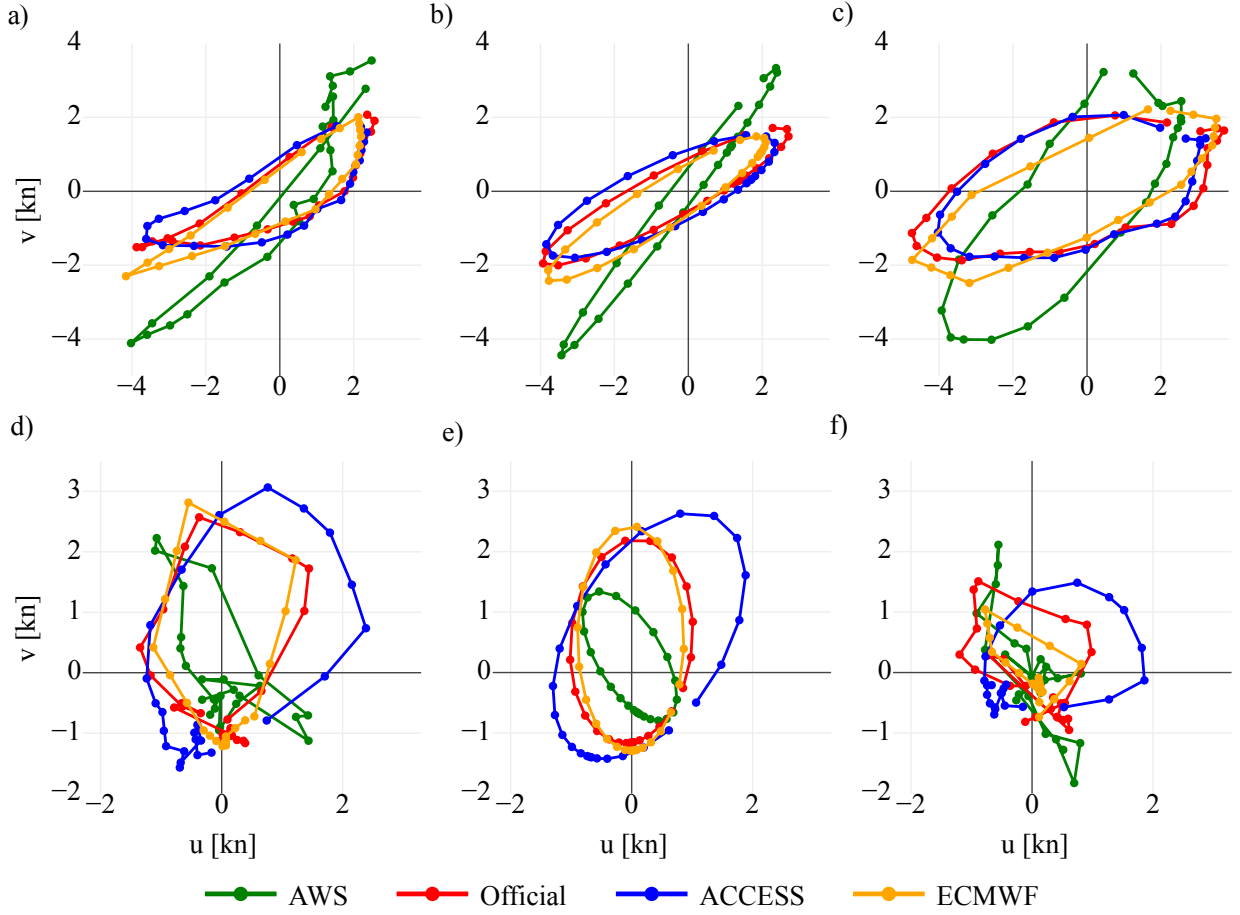


FIG. 13. Ellipse fits. Could instead just provide one example.

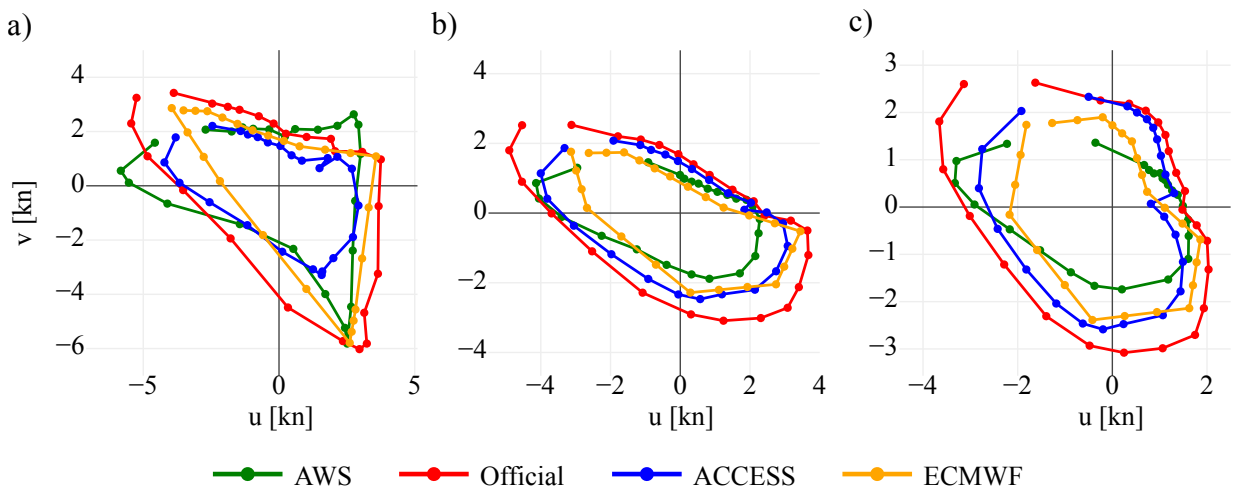


FIG. 14. Ellipse fits. Could also include the ellipses, but this makes the figure very large.

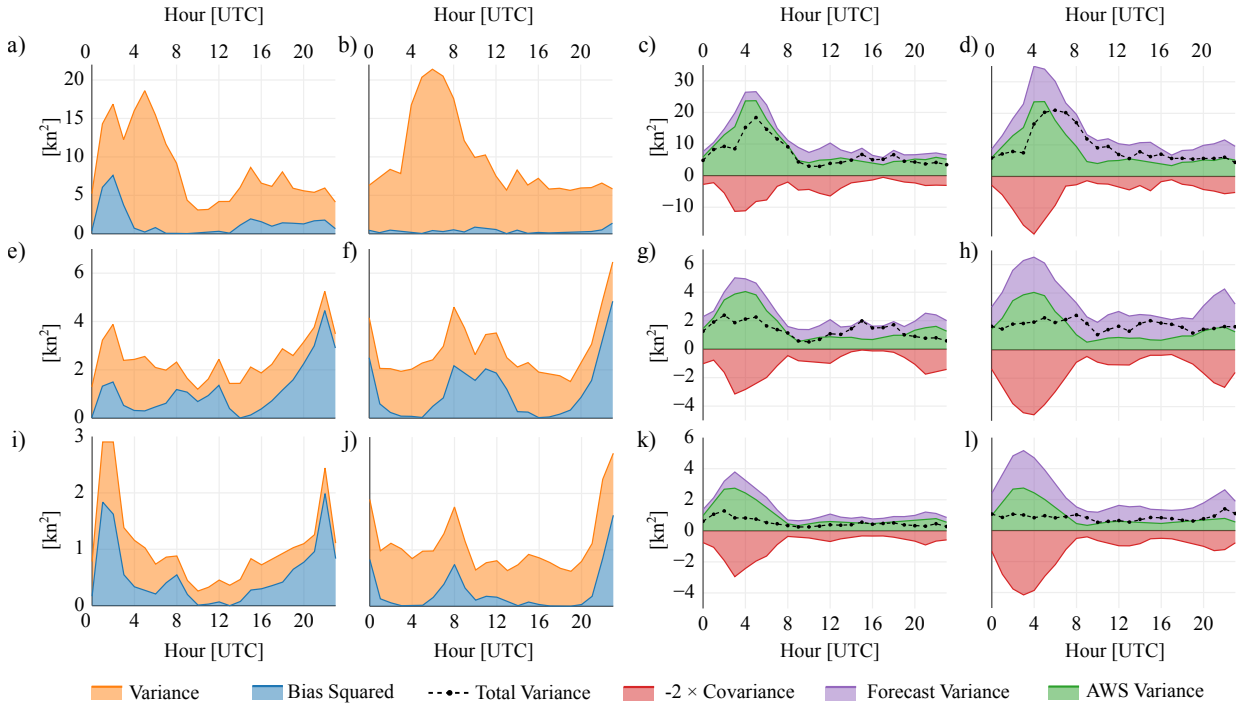


FIG. 15. Actual perturbation standard deviation values. Note that official performs the worst at this scale!

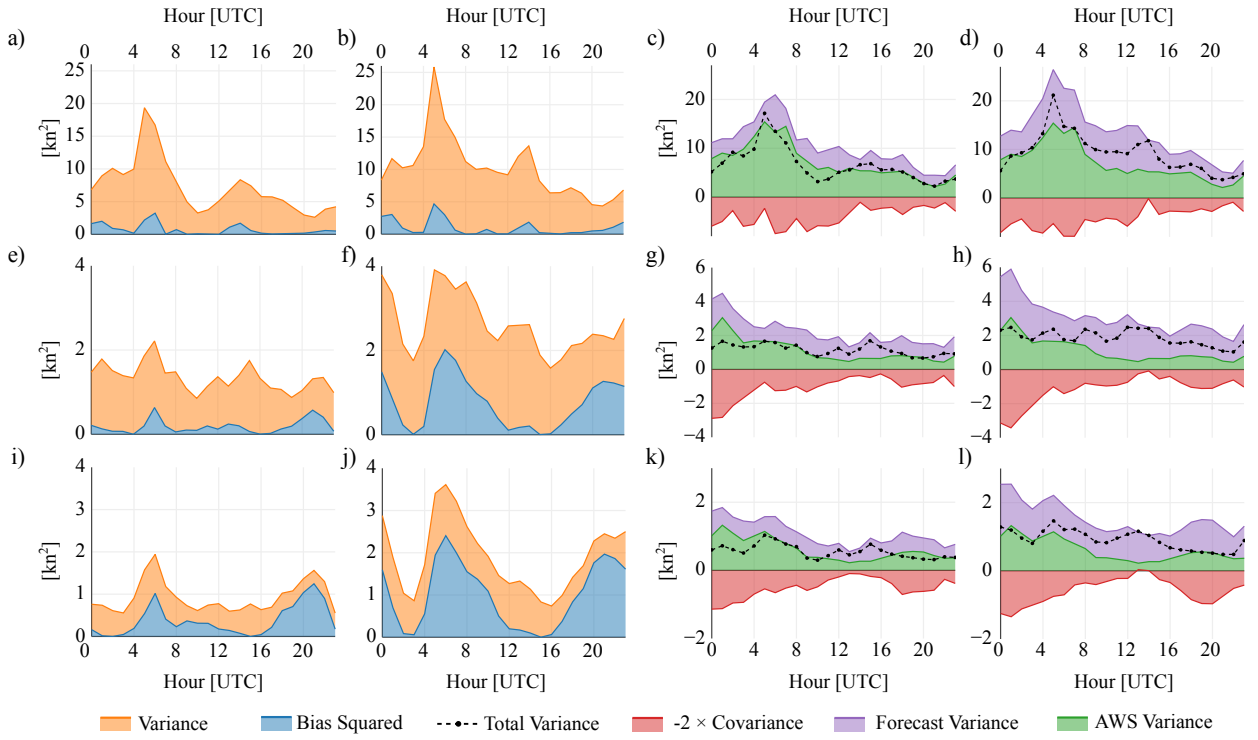


FIG. 16. Actual perturbation standard deviation values. Note that official performs the worst at this scale!